State of the Art Review on Membrane Surface Characterization: Visualisation, Verification and Quantification of Membrane Properties

Daniel J. Johnson, Nidal Hilal[*]

Centre for Water and Environmental Research (CWATER), College of Engineering, Swansea University, Swansea SA28PP, United Kingdom

** Corresponding author, email: N.Hilal@swansea.ac.uk*

Abstract

Many of the properties exhibited by separation membranes are due to interactions at the interface with their environment, including flux, rejection of solutes and surface fouling. As such when trying to understand how such interactions affect their function and when developing novel membranes with improved properties, a thorough understanding of their surface properties is essential. In this review paper we describe and discuss a number of instrumental techniques commonly used to characterize membrane surface, along with illustrative examples from the literature on membrane development and characterization. The techniques described include spectroscopic techniques, microscopic techniques and methods to measure the surface wettability and electrokinetic behaviour.

Keywords

Surface characterization, membrane fouling, membrane development, fouling, spectroscopy, microscopy, wetting, electrokinetics.

Table of Contents

1.0 Introduction

As all interactions between filtration membranes and the surrounding medium, containing a potentially diverse mixture of water, ions, organics and macromolecules, occur at the surface, it follows that the physical and chemical properties play a fundamental role in their operation, affecting membrane flux, rejection and fouling. As such, when trying to understand the interactions underpinning these processes, or when developing new improved membranes, characterisation of the pertinent membrane surface properties is very important. This review will attempt to summarise the major techniques used for investigation of membrane surface properties. In the first section we will examine spectroscopic techniques, those which use electromagnetic radiation. Fourier transform infra-red spectroscopy (FTIR), particularly with the attenuated total reflectance module (ATR), is one of the most important techniques available to the membrane developer to understand chemical modifications made to membrane surfaces. The several modes of Raman spectroscopy can not only complement the chemical information of FTIR, but can add structural information and is often combined with imaging techniques to allow surface mapping of these properties. X-ray photoelectron spectroscopy (XPS) is an extremely powerful technique to examine the elemental composition of surfaces. Other techniques, including nuclear magnetic resonance (NMR), small angle X-ray / neutron scattering (SAXS/SANS) and electron spin resonance (ESR), whilst not strictly surface

techniques, are included due to their great utility in obtaining information on the effects of surface treatment and modification into the structures in the upper active layer of membranes. The next section deals with three high resolution microscopy techniques, atomic force microscopy (AFM), scanning electron microscopy (SEM) and transmission electron microscopy (TEM). AFM allows quantitative examination of three-dimensional structures of surfaces in fluid environments and can generate a wide range of quantitative information on surface morphology, surface nano-mechanical properties and interaction forces between the surface and other materials. Electron microscopy techniques, SEM and TEM, are almost ubiquitous as a technique to gain high quality, high resolution images of membrane surfaces and cross-section, and when combined with energy dispersive X-ray detection (EDX) can simultaneously obtain elemental information. We examine several techniques for determination of surface wetting properties through measurement of contact angle at the air-water-solid interface. Finally, we look at membrane surface electrokinetic properties and techniques to determine surface electrical potential.

2.0 Spectroscopic Techniques for Characterisation of Membrane Surfaces

2.1 Fourier Transform Infra-Red Spectroscopy (FTIR)

2.1.1 Introduction and basic principles

Much research and development on the development of separation membranes is on the creation of new surface chemical functionalities in the search for membranes with increasing resistance to fouling. One of the most mature and widely used technologies to investigate chemical functionality of surfaces is the group of related spectroscopic techniques termed Fourier Transform Infra-Red spectroscopy (FTIR).

As with all infra-red spectroscopy techniques, FTIR probes the vibrations of molecular bonds. This is because infra-red (IR) frequencies (approximately 10^{12} to 10^{14} Hz) overlap with molecular vibration

frequencies. A molecular vibration is a movement of atoms within a molecule which involve no rotation and do not alter the centre of mass of the molecule. If the frequency of IR radiation is identical to that of a particular molecular vibration, then it can cause the vibration to move to a higher energy state. The vibrations may include stretching (both symmetric and asymmetric, and bending (in plane or out of plane), referred to as 'normal' modes.

FTIR instruments provide results much faster than traditional IR spectrometers. Inside the instrument a black-body source emits a beam of IR radiation. This beam is passed through an interferometer where different beams with different path lengths are combined to create constructive and destructive interference. This interference pattern, is termed an interferogram. As the beam is passed through the sample and wavelengths of IR light are absorbed in a manner specific to that sample then the interferogram will be in turn characteristic of that sample. This can be plotted as an interferogram of energy versus frequency. Finally, computer software subtracts a reference (background) signal from the sample interferogram by Fourier transform to produce the sample spectrum.

The vast majority of FTIR instruments fall into one of four categories: transmission, attenuated total reflectance (ATR), diffuse reflectance spectroscopy (DRIFTS) and specular reflectance/ reflection-absorption [1, 2]. The simplest, from an operational perspective and oldest technique is simple transmission. Here a beam of IR light is passed through the sample and the transmitted energy is detected and used to produce the resultant spectrum.

ATR-FTIR is useful for examining sample surfaces, rather than bulk materials and so is of especial interest for study of chemically modified membrane surfaces. This technique typically requires an add-on module to the FTIR instrument. During ATR-FTIR operation a beam of IR light is directed onto a high refractive index crystal, which may typically be germanium, zinc selenide, diamond, thallium – bromoiodide or silicon, placed in direct contact with the sample (see figure 1). Multiple internal reflections of the IR beam are produced, which creates an evanescent wave, which interacts with the

material of the sample. Absorption of the evanescent wave by the sample leads to its attenuation, before being reflected back through the crystal and onto the detector [2].

<Insert figure 1 here>

DRIFTS is useful for the study of particulate samples. The DRIFTS technique uses true diffuse reflectance where the incident beam can be either reflected off the surface of one or more particles in many directions without penetrating the surface, or may penetrate and be scattered [2]. Here IR energy is channelled into a sample chamber filled with sample particles suspended in a material, such as KBr, which is transparent to IR radiation. The scattered and diffused incident bean is collected by a mirror which reflects it onto the detector. The detected IR radiation is then processed as with other FTIR techniques. True specular reflectance is unique in that it measures reflected IR radiation rather than IR absorption. It utilises the variance of the unique refractive index for every material with the wavelength of the light being reflected.

FTIR instruments typically operate in the middle of the IR range, with wavenumbers of approximately 666 to 4000 cm^{-1}. In this region, the transition energies for many functional groups' vibrational states can be found within this range. As a result, the presence of specific absorption bands can be used to identify the presence of the corresponding functional groups.

The vibration of whole molecules produces complex absorption patterns at high frequencies, which is often particular to that chemical and hence is of great utility in identifying particular molecules. Single, double and triple bonds are also seen in different parts of the IR spectrum, typically appearing in the 2500-4000 cm^{-1}, 1500-2000cm^{-1} and 2000-2500cm^{-1}, respectively.

2.1.2 Studies of Membrane Surface Chemical Modification

A number of different techniques have been used to modify the surfaces of membranes to change their functionality in some way. FTIR based techniques are a powerful tool in assessing the functional groups present in the membrane and are of great utility when modifying membranes. Surface modification may take the form of surface coating, treatment with chemicals or plasma,

surface grafting of chemical species, enzyme immobilisation, UV induced modification and addition of nanostructured fillers.

A common approach in the creation of membranes for water treatment application is by blending of complimentary polymers together. This can provide blended polymer membranes with useful properties which may not be found in membranes consisting of single polymers [3-6]. These properties may include higher permeability and higher selectivity leading to improved performance for desalination, gas separation, wastewater treatment and other separation applications [3, 4, 6-8].

Mannan *et al* developed polysulfone / polyether sulfone (PSF/PES) membranes for CO2 separation applications [3]. Observation of the FTIR absorbance spectra showed absorbance peaks shifting in frequency (see figure 2). The authors noted the presence of a broad peak with a wavenumber of between 3448 and 3460 cm^{-1} which was ascribed to the presence of hydrogen bonding between the PSF and PES, although these peaks are not easily discerned in the published figure. This demonstrated that the PES and PSF polymers were compatible, with positive physical interactions occurring between them.

<insert figure 2 here>

Chemical modification of membrane materials by the addition of functional groups is commonly carried out by oxidation, hydrolysis, addition and substitution. Oxidising agents including chromic and nitric acid, and potassium permanganate, may be used to oxidise the membrane surface by the introduction of oxygen radicals. For instance, Bottino and colleagues [9] modified poly(vinylidene fluoride) (PVDF) powder with potassium permanganate. Membranes created using the modified PVD showed improved pure water flux and increased hydrophilicity compared with unmodified PVDF membranes. ATR-FTIR showed the appearance of a new absorption band with a peak at 1650 cm^{-1}. The authors attributed this band to the formation of carbonyl bonds formed as a result of dehydrofluorination and oxidation reactions.

Modification can also be carried out on pre-fabricated membranes. This allows changes to be made to the active surface of the membrane without altering properties of the bulk of the membrane

material, for instance avoiding weakening of the mechanical properties of the membrane [10]. Plasma treatment of membrane surfaces has this advantage, allowing membranes with surface layers of low hydrophobicity to be created, without weakening the strength of the membrane matrix.

<Insert figure 3 here>

Plasma treatment can add a large variety of oxygen containing groups to the membrane surface, which can facilitate the interaction and bonding to the surface of a variety of chemical groups to create membrane surfaces with specialised properties [11]. Bae *et al* [12] used ATR-FTIR to study the effects of Freon-116 plasma treatment on the surfaces of polypropylene (PP) membranes. In figure 3 is shown the obtained ATR-FTIR spectra of the polypropylene membranes after being exposed to the Freon-116 plasma for different durations. The bands which can be seen at 1300 cm^{-1} were attributed to C-F bond stretching. The authors attributed the increasing intensity of this band with increased plasma exposure time to the increased number of C-F bonds on the membrane surface, replacing C-C and C-H bonds. The new C-F bonds were explained as being formed from carbon radicals on the membrane surface, generated by the plasma, and carbon atoms in the Freon-116 molecules. Wavhal and Fisher [13] used transmission FTIR to study the grafting of polyacrylic acid (PAA) onto PES membranes using Argon plasma (see figure 4 for reproduced FTIR spectra). As the plasma will penetrate into the whole of the membrane, the authors used transmission mode FTIR to study the chemical changes to the bulk membrane material. They observed a new absorption band appearing at approximately 1725.5 cm^{-1} which was attributed to the presence of PAA on the membrane surface. As the grafting yield (mass of grafted material per unit area) was increased, this absorption band increased in intensity and became resolved into two peaks. This was attributed by the authors to intra- and inter-chain interactions between carboxylic groups.

<Insert figure 4 here>

Modification of polymer membrane surfaces using ultraviolet (UV) treatment can also be monitored using FTIR. For instance, Garcia-Ivars *et al* [14] used UV radiation for the surface photo-modification of PES membranes. This gave rise to a new absorption peak at 1645 cm^{-1}, which was ascribed to carboxyl groups.

<Insert figure 5 here>

Covalent attachment of macromolecular chains to the functional end groups of polymers by surface grafting is another common technique to change the surface properties of membranes. Commonly three approaches are used, which are: photo-induced grafting, radiation induced grafting and surface initiated atom transfer radical polymerization (ATRP) [15, 16]. Modification of PVDF membrane surfaces by grafting of poly(N-isopropylacrylamide) (PNIPAAm) was reported by Zhao and Chen [17]. ATR-FTIR absorption spectra are shown in figure 5. Comparison of the spectra before and after modification can show clearly the effect of the modification on the chemical groups which are present at the surface. After grafting of PNIPAAm two new absorption peaks are seen to arise at 1540 and 1620 cm^{-1}. These were attributed by the authors to N-H stretching of amide groups and secondary amide C=O stretching in the PNIPAAm.

As well as attaching macromolecule chains, grafting of more complex macromolecules, such as enzymes, has also been reported. These proteins may be adsorbed onto the membrane surface by several mechanisms, including physical or chemical binding, incorporation on a polymer gel matrix or by electrochemical attachment [10]. The efficient chemical activity of enzymes, such as proteases and lysosyme, have been reported as being effective in the hydrolysis of structural components in biofilms formed by microbial action [18-21]. Hanušová *et al* [22] showed that the formation of covalent bonds between both glucose oxidase and lysozyme with a polyamide surface showed a shift in the position of bands characteristic of the structure of the enzymes. As a result, it has been suggested that alterations in the position of spectral peaks can be a sign of enzyme attachment to membrane surfaces [22, 23].

Incorporating organic and inorganic nanoparticles into the structure of polymer membranes is a way of changing physicochemical properties of membranes to improve their performance [24-27]. Mohammed *et al* [28, 29] fabricated photocatalytic membranes for treatment of waste water containing TiO_2 nanoparticles. By comparing the FTIR spectra of the modified and unmodified membranes it was observed that a slight shift in absorption peaks for O-H stretching decreased in intensity. The authors attributed this to the interaction between the O-H groups and the Ti-O bond of the nanoparticles. Similarly, other researchers used FTIR to study incorporation of Al_2O_3 nanoparticles into photo-modified PES membranes [14]. This resulted in the creation of three new peaks in the FTIR spectra not present in the PES membrane, demonstrating successful incorporation.

2.2 Raman Spectroscopy

2.2.1 Introduction and Basic Principles

Raman spectroscopy is a technique complementary to IR spectroscopy. Here a beam of monochromatic laser light, with frequency ranges varying from the visible to near UV, is passed through a sample. It is sensitive to molecular vibrations, rotations and other low frequency modes and can provide useful information on the crystalline structure of polymers and other macromolecules. Interaction between the laser light and molecular excitations result in an energy shift which provides information about the vibrational modes the light has interacted with. As a result, Raman can provide both qualitative and quantitative information on polymer functional groups and structure and also on their conformation and orientation [30, 31].

Raman spectroscopy relies upon the Raman effect, which is the inelastic scattering of light due to an exchange of energy between photons in the light beam and the vibrational energy levels of the molecule it has collided with, leading to the scattered photon having a different energy level to the incident photon. Dependent upon the nature of the interaction, the scattered light may have a higher or lower energy than the incident light, although it is mainly the higher energy scattered light which is studied [32]. The Raman spectrometer consists of a light source, a monochromator, a

sample holder and a light detector. The scattered light becomes dispersed by frequency and is used to construct a Raman spectra. It is complementary to IR spectroscopy as it is sensitive to some modes which are not easily detected by IR and vice versa [33].

There are a number of modes of Raman spectroscopy which have been developed to increase the sensitivity of the technique and enhance resolution. The two most prominent of these techniques are tip-enhanced Raman spectroscopy (TERS) and surface-enhanced Raman spectroscopy (SERS). TERS, first reported by Stöckle *et al* [34] works on the principle that when a sharp metal probe is scanned across the sample surface in conjunction with a beam of monochromatic light then the Raman signal is enhanced, with it being possible to obtain a Raman spectra with a high degree of spatial resolution in conjunction with surface topography [35]. SERS, on the other hand, improves the Raman signal by deposition of a sample onto a suitable SERS active substrate, which may be a rough metal surface, a nanostructured surface or colloidal particles, which leads to excitation of localised surface plasmons, enhancing the Raman signal [36].

Raman spectroscopy can also be combined with microscopy techniques, for instance for Raman confocal microscopy [37], combined confocal Raman and AFM [38] and combined depth profilometry with Raman spectroscopy [32]. Such techniques allow a much greater amount of information to be captured by combining imaging with the capabilities of Raman spectroscopy. It also allows the collection of Raman spectra from specific sites on samples to gain structural information at fine resolution. The combined techniques are useful for investigation of the surface structure of membranes and study of the fouling of surfaces.

2.2.2 Characterisation of Polymer Membranes and Membrane Formation

Orientation in polymer membranes can typically result from the production techniques, including using a casting knife for flat sheet membranes or by spinning in the case of hollow fibre membranes. This orientation of the polymer membranes, as well as any crystallinity and other structural elements, can be investigated using Raman techniques [33]. As the macroscale characteristics and performance of a material can be related to the internal structure, then obtaining an understanding

of the internal structure and how production conditions affect it can give insight into transport mechanisms during operation and the mechanisms which cause particular structures to form during fabrication. In particular study of the active layer of the membrane (typically the upper few microns) is of interest as this section determines membrane selectivity and fouling. Raman spectroscopy allows the direct study of polymer chain orientation and polymer crystallinity, allowing such factors to be studied during membrane fabrication itself [39].

Menut *et al* [40] used Raman confocal spectroscopy (RCS), in conjunction with FTIR and other techniques, to study formation of a liquid layer on the top surface of membranes made using vapour-induced phase separation technique (VIPS), working with a blend of poly (ether-imide) (PEI) and *N*- methyl pyrrolidone (NMP). RCS was used to determine the film thickness during membrane formation in dry and humic air, as well as the mass ratio of the NMP/PEI at the air-liquid interface. This allowed changes in the polymer composition of the active layer during the membrane formation process to be directly monitored, allowing some insight into the mechanisms of active layer formation to be obtained.

The high spatial resolution of Raman spectroscopy allows point-by-point mapping of the cross sections of membranes made using a blend of PVDF with polyvinylpyrrolidone (PVP) as an additive [39]. The PVP concentration profile across the cross sections were determined by assigning peaks at different sections of the Raman spectrum to PVDF and PVP. A linear dependence between the peak intensity ration and PVP concentration was found allowing the construction of a calibration curve. This calibration curve was then used to determine the mass fraction of the PVP at specific points through the cross section.

Cross sectional analysis combined with Raman microscopy was used to perform an analysis of the degradation of polypropylene (PP) hollow fibre membranes used in microfiltration applications [41]. The samples examined had become degraded after several days use as a pre-treatment stage in a military water purification system. Raman spectra on cross sections of the membranes showed the appearance of a new peak at ~170 cm^{-1} in degraded samples, when compared with a pristine

membrane. This peak was assigned to carbonyl –C=O aldehyde stretching groups. Another new peak at ~3450 cm^{-1} was also seen for only some membranes, which was assigned to –OH bonds. This confirmed observations made with other techniques suggesting that the membranes had become oxidised. These peaks were only seen at scans at the upper and lower parts of the cross sections, suggesting this was largely a surface oxidation.

2.2.3 Study of Fouling using Raman Spectroscopy

Several studies have been made utilising SERS when studying the phenomenon of membrane fouling. For instance, Lamsal *et al* [42] studied pristine, organically fouled, and cleaned membranes, which showed different SERS spectra. This showed that it is possible to differentiate the different functional groups present in organic membrane fouling (see figure 6). The three membrane samples showed markedly different SERS spectra, compared with conventional Raman which was unable to differentiate the three samples, presumably as it was largely probing the bulk membrane material rather than surface chemistry.

SERS was also used to study the formation of a biofilm on a cellulose ester membrane surface [43], using two model bacterial species (*Brevundimonas diminuta* and *Staphylococcus aureus*). This allowed characterisation of the changes in dominant species over time – *S. aureaus* was dominant in the first 8 hours of biofilm formation, but was later largely replaced by *B. diminuta*. Furthermore Patel *et al* [44] demonstrated it is possible to combine SERS with multivariate statistical analysis to distinguish bacterial species, and even strains.

<insert figure 6 here>

2.3 Nuclear Magnetic Resonance Spectroscopy (NMR)

2.3.1 Introduction and Basic Principles of NMR spectroscopy

The technique of NMR first emerged from the work of Bloch *et al* [45] and Purcell *et al* [46] reported in 1946, whilst working independently of each other. Some isotopes when exposed to an external magnetic field see a split in the energy levels of their nucleons, according to the spin states available,

with the lowest energy state (spin-aligned) being the most populous. When these nuclei are further exposed to radio waves of specific frequencies they may become flipped from a low energy state to a high-energy state, by absorbing energy [47]. Each type of nucleus has a characteristic spin. For instance, ^{1}H, ^{15}N, ^{19}F, ^{31}P have a spin of ½, whereas ^{12}C, ^{16}O and ^{28}C have no net spin and thus can't be probed using NMR [48]. The energy absorbed is dependent upon the spin properties of the atoms and the applied external magnetic field. The data recorded by an NMR instrument is the chemical shift, which is the difference between the resonant frequency of the atoms being probed and that of a standard. Chemical shift is reported in units of parts per million or ppm [49].

As the chemical shift is not just dependent upon the nuclei, but upon their environment, such as proximity to other nuclei, this technique allows the probing of structural relationships, either statically or over a wide range of timescales [50]. Most commonly ^{1}H and ^{13}C spectra are used.

2.3.2 Membrane Structure and Morphology Prediction by NMR

<insert figure 7 here>

One of the potential applications of NMR spectroscopy of interest in membrane fabrication and development is the investigation of polymer blend miscibility. Rana *et al* [51] produced membranes, which were produced from blending cellulose acetate (CA) and poly(2,6-dimethyl-1,4-phenylene oxide) (PPO), and incorporated 2,2,6,6-tera-methyl-1-piperidinyloxy (TEMPO) as a spin probe. Using solid state ^{13}C NMR they concluded from their results that the TEMPO had no chemical or physical interaction with the CA. PSF membranes containing functionalised carbon nanotubes were investigated by Nechifor *et al* [52] using ^{1}H NMR spectroscopy (see figure 7 for an example NMR spectrum). Their results demonstrated a number of spectral shifts, including ones at 2.975 and 2.977 from NH protons attributed to the amine functionalised carbon nanotubes. It was concluded that the CNTs were miscible with the PSF matrix of the membrane.

2.4 Electron Spin Resonance / Electron Paramagnetic Resonance Spectroscopy

2.4.1 Introduction and Basic Principles of Electron Spin Resonance Spectroscopy

Electron spin resonance (ESR) spectroscopy, also known as electron paramagnetic resonance (EPR) and electron magnetic resonance (EMN) spectroscopy, is a technique for probing atoms and molecules containing stable unpaired electrons. It is roughly analogous to NMR spectroscopy, but whereas NMR probes the magnetic moments of nuclei ESR probes the magnetic resonance of electrons in paramagnetic materials.

When an external magnetic field is applied to a material, the magnetic moments of any atoms containing unpaired electrons is aligned either parallel or antiparallel to the magnetic field, depending on the spin states of the electrons. Although the requirements for having unpaired electrons may seem limiting, there are a large number of molecules which satisfy this criteria, including transition metals, organic and inorganic free radicals, molecules in electronic triplet states, semi-conductor impurities, electrons in unfilled conduction bands and electrons in materials damaged by radiation [53]. For samples which are not paramagnetic, a ‘spin label’ or ‘spin probe’ can used, which typical consists of adding a free radical o some sort to the material, typically a nitroxide radical.

Electrons have two kinds of magnetic moment: orbital magnetic moment from motion around the atomic nucleus and spin magnetic moment, from the electrons rotation about its own axis. Under no applied external magnetic field these two spin states have equal energy. When a magnetic field is applied, the electrons will be induced to spin in the same (up) or opposite (down) direction to the applied field, each with different energies. When electromagnetic radiation is applied to these atoms then a change in the spin state may be induced. This change is dependent upon both the wavelength

of the radiation and the strength of the magnetic field and also the interactions between the electrons and their local environment. As a result an absorption spectra can be obtained for a particular material which will provide information on structural and dynamic information about chemical and structural properties of a material [33].

2.4.2 Study of Polymer Membranes using ESR Spectroscopy

Khulbe *et al* [54] reported studies of polymer membranes made using polyphenylene oxide (PPO). PPO powder was determined to contain free radicals, which are included in membranes fabricated from the powder form. Due to a low signal from these radicals they undertook to make further measurements by including TEMPO as a spin label [55]. Membranes were studied containing PPO, TEMPO and a trichloroethylene solvent, with measurements being taken as the solvent evaporated at different temperatures. Signal intensity decreased with evaporation temperature, with intensity reaching zero for the lowest temperature measured. The authors suggested that this behaviour could be due to a crystalline state or other molecular ordering occurring in the membrane at the low temperature. Khulbe *et al* also used the TEMPO probe to study the structure of the active layer of CA membranes designed for RO applications [56]. They found from their measurements that the pore sizes increased at low temperatures; that void spaces within the membrane were reduced in the absence of swelling agents in the casting solution; and that the void space was also reduced when the membrane was dried.

The used of spin probes can also be used to study membrane transport mechanisms by including the probe in feed-water solution, or immersing the membranes in a solution containing the spin probe [57, 58], rather than by including it in the casting mixture.

2.4.3 Study of Membrane Fouling using ESR Spectroscopy

Oppenheim and colleagues studied fouling of PSF ultrafiltration membranes using spin labelled bovine serum albumin (BSA) and hen egg lysozyme (HEL) [59]. When filtering a solution containing

the larger BSA protein (65k Da) through a 100,000 molecular weight cut-off (MWCO) PSF membrane the majority of the protein uptake occurred in the initial 10 minutes, apparently independent of solution properties (pH, salt concentration). It was concluded that the initial solute build up was likely a result of pore blocking, rather than surface adsorption. Further measurements were carried out using HEL solutions (15k Da) with tighter 10,000 and 30,000 MWCO membranes. Spectra for the two membranes were reported to be significantly different. It was concluded that for the 10,000 MWCO membrane only surface adsorption was occurring as HEL is rejected by this membrane, but for the 30,000 MWCO membrane a mixture of surface adsorption, pore plugging and pore adsorption was occurring. However, the mechanism by which this will lead to such different spectra is unclear.

Kulbe *et al* [33] also used BSA as a model foulant in studies of protein fouling of ultrafiltration membranes made of PES containing PVP additive, both with and without a TEMPO spin probe. The authors concluded that BSA was deposited in the membrane surface and within pores in specific orientations, that the packing density of BSA in pores depends on both the pore size and the feed pressure, and that the fouling depends on the structure of the solute.

2.4.4 Study of Membrane Degradation using ESR

Oliveira *et al* used ESR to study the degradation and structural alteration of polyamide (PA) nanofiltration membranes by hypochlorite [60]. Hypochlorite solutions are regularly used for removal of membrane fouling and have been previously implicated in damage to membrane surfaces [61, 62]. Several factors were examined which may affect degradation, including hypochlorite concentration, pH, light intensity and irradiation [60]. As would be expected the concentration of cleaning agent had a direct effect on the number of free radicals active at the membrane surface, as did the solution pH. The particular radical species which were present could not be identified, however, due to a lack of ‘hyperfine’ detail in the ESR spectra.

2.5 X-Ray Photon Spectroscopy

2.5.1 Introduction and Basic Principles

X-ray photon spectroscopy (XPS) is a quantitative surface analytical technique which provides information on the elemental composition information. XPS works on the principle that when a surface is bombarded with electromagnetic energy of sufficient energy then a finite number of the surface atoms will absorb a photon and emit an electron, a phenomenon called photo-emission. Electrons will have a kinetic energy which is equal to the difference between the energy required to remove the electron from its orbital (binding energy) and the energy of the absorbed photon [63]. It is these ejected electrons and their kinetic energy which is detected by this technique. Data is typically plotted as binding energy on the *x*-axis versus the intensity on the *y*-axis, with the binding energy within the range of 0 to 1200 eV. The binding energy for each peak is typically characteristic for a particular element, although the chemical state of the emitting atom may have an effect on the binding energy and shape of the peak, giving some information on chemical bonding state. For atoms within the bulk material which may become excited, the kinetic energy of any emitted electrons is attenuated by collisions with other atoms to the point that they either do not escape the surface or have too low an energy to be detected.

Peaks may appear different depending upon the orbitals from which the ejected electrons originate: s orbitals present single peaks and are relatively straightforward to interpret. However electrons from p, d and f orbitals may present multiple peaks. This multiplet splitting occurs when a vacancy in a core orbital due to photoionization leads to coupling with an unpaired electron in the outer shell. A variety of final states may occur and be seen in the resultant spectrum [64].

2.5.2 Investigation of Polymer Membranes with XPS

The XPS technique was utilized by Ariza and co-workers [65] to compare a laboratory fabricated membrane (B0) with a commercially produced nanofiltration membrane (NF45). Both membranes were polyamide / polysulfone composites, with the active layer consisting of polyamide (≤ 1 μm),

with the polysulfone as a porous support. As a result, the XPS technique probed the polyamide layer alone for both membranes, with the main elements characterised being C, N and O (see figure 8). The NF45 membrane exhibited a low proportion of contaminants, seen from a small proportion of S (atomic concentration < 0.5%) and a slightly higher O reading than expected. The B0 membrane showed some S and P elements (<0.5 %) and Cl (<1 %) as well as lower O and greater N than would be expected from the theoretical value for polyamide. The authors interpreted this as showing that the B0 membrane had contamination from solvents and washing agents which had not been excluded from the membrane during fabrication. The authors also used XPS to study the composition at different depths into the polyamide layer by adjusting the angle of the X-ray beam. The profile of NF45 was very homogenous, except for a slight difference at depths of < 3nm, where aliphatic O and C rich groups were observed, indicating surface contamination. B0 was also very homogenous, again except for surface contamination.

<insert figure 8 here>

The incorporation of aluminosilicate single wall nanotubes (SWNT) into thin film nano-composite (TFN) membranes with poly (vinyl alcohol) (PVA)matrices was studied by Barona *et al* using XPS as one of a battery of characterisation techniques [66]. The intensities of C(1)s (284 eV) and O(1)s (532 eV) peaks were used to determine the relative elemental composition of the upper 10 nm of the TFN membrane, along with Al and Si. Increasing concentrations of Al and Si were seen at increasing concentrations of SWNTs, demonstrating their incorporation into the surface PVA layer.

Wei *et al* [67] used XPS to characterise a plasma treatment using CF_4 of PES membrane surfaces. Scans revealed that the content of fluorine on the membrane surface increased from 0 % before plasma treatment to 50.8 %, becoming the dominant elemental component. This demonstrated a strong fluorination effect, making the surface layer more hydrophobic.

2.6 Small Angle Neutron Scattering / Small Angle X-Ray Scattering (SANS / SAXS)

2.6.1 Introduction and Basic Principles of SANS /SAXS

Small angle scattering spectroscopic techniques using neutron (SANS) and X-rays (SAXS) are used for the characterisation of membrane structures at length scales typically in the nanometre range. SAXS is sensitive to electron density, whereas SANS involves neutron interaction with nuclei. When using hydrogen containing polymers in a solvent containing deuterium instead of hydrogen a higher degree of sensitivity can be obtained due to the different neutron scattering lengths between hydrogen and deuterium. This makes SANS better suited than SAXS for examination of polymer compounds with low electron density [68].

The intensity of SAXS and SANS can be written in simplified form as a function of a scattering vector, Q which is dependent upon the wavelength and scattering angle and the forward scattering intensity I(Q) [69].

2.6.2 Structural Investigations of Polymer Membranes using SANS / SAXS

Singh and Aswal [68] used SANS to probe the nanoscale structures of thin film composite (TFC) RO and NF membranes consisting of a polysulfone support layer covered with a polyamide selective layer (≤ 0.2 μm thickness). The researchers examined both membranes and thin films of the polyamides which were put into water and broken up to form a colloidal dispersion. The SANS study of these membranes allowed measurement of the sizes of the nanoscale building blocks of the polyamide layers as having a sphere median radius of 118 Å for the RO membrane and 106 Å for the NF membrane.

Singh *et al* [70] used SANS to compare two different membranes fabricated from poly dimethyl siloxane (PDMS), intended for treatment of water contaminated with volatile organic compounds. For both membranes cross-linking in the liquid state caused an increase

in the volumes occupied by the macromolecules, which then reduced during solvent evaporation.

3.0: Microscopy Techniques

3.1 Atomic Force Microscopy (AFM)

3.1.1 Introduction and Basic Principles

Atomic force microscopy is one member of a family of microscopic techniques collectively referred to as scanning probe microscopy (SPM). It uses a sharp probe, mounted on a flexible microcantilever arm, which physically interacts with the sample surface to obtain high resolution images of surface topography. It can also be used to probe interaction forces between the probe and the surface, leading to measurement of nano-mechanical surface properties, adhesion forces and long range interaction forces. It does not require vacuum, allowing measurements to take place in air and liquid environments and does not require conductive samples or surfaces to be metal coated.

In essence, the sharp imaging tip is scanned across the sample surface in three dimensions by use of piezo crystals which are ether associated with the sample holder or probe holder, depending upon the particular instrument. The configuration of the piezo also varies, with some instruments using a tube shaped piezo crystal, which flexes to produce *x*, *y* movement or extends / retracts to produce movement on the *z* axis. Alternatively, separate piezos may be employed for each axis of movement. Deflection of the cantilever is detected by an optical lever system, where a beam of laser light is reflected from the upper side of the cantilever onto a position sensitive photodetector.

There are now a large number of imaging modes available for specific application, many of which are proprietary and instrument manufacturer specific, but there are three basic modes most commonly

used: contact mode, tapping mode and non-contact mode, with the latter two sometimes referred to as dynamic modes. The primary data obtained are high resolution three-dimensional scans of the surface topography (the height image). From this quantitative information may be obtained including changes to morphology due to fouling or chemical modification and in some cases the diameter of pore openings and porosity [71-78].

Contact mode is the simplest operating mode. Here the probe maintains constant contact with the sample surface. As the probe is raster-scanned across the surface and encounters features of different heights the flexure of the cantilever will change. A feed-back loop is employed to keep the deflection of the lever, and hence tip-sample interaction force, at a constant set-point by extending or retracing the piezo. As the tip is raster scanned across the surface, the change in *z*-position needed to maintain constant deflection allows an image of surface height to be built up to high precision. A map of frictional forces may also be built up by monitoring the lateral deflection of the lever simultaneously with acquisition of height data [79-81].

Tapping mode, also sometimes referred to as intermittent contact or amplitude modulation mode, is likely the most commonly used AFM mode. It was developed to overcome some limitations of contact mode, which include high imaging forces (normal to the surface) and lateral forces when encountering edges etc., which can decrease resolution when imaging soft or rough samples [82-84]. Here the cantilever is driven to oscillate at a frequency close to resonance, allowing the imaging tip to briefly engage with the sample before disengaging. As the height of the sample varies the tip is engaged with the sample for a greater portion of its cycle, leading to a decreased oscillation amplitude. By moving the probe in the *z*-direction the oscillating amplitude may be maintained at a constant set-point, as well as recording height information in a similar manner to contact mode. In addition to changing the amplitude, interaction with the surface changes the oscillating frequency. The phase change between the drive and oscillating frequencies, the phase signal, is dependent upon various properties of the tip sample interaction, including interaction force, mechanical compliance of the surface, adhesion forces etc. This makes it extremely useful for highlighting

different surface domains, surface pores and other features which may not be clearly seen in the height image, although due to the large number of factors affecting the phase signal it is difficult to obtain quantitative information [85, 86].

A variation on tapping mode, which is useful for obtaining quantitative nano-mechanical information simultaneously with sample topography, is peak force mode [87, 88]. Here the oscillating frequency is much lower than the resonance frequency, allowing individual probe-sample interaction events to be measured as force curves. From features on the force curves, properties such as adhesion and sample deformation can be directly measured and further fed into models to estimate elastic modulus.

Non-contact mode is another dynamic mode frequently seen in the literature. The cantilever is oscillated at much smaller amplitudes than is used for tapping mode. Instead of amplitude, frequency is used as the feed-back signal. As the frequency shifts due to long range interaction forces, the probe may be kept in close proximity with the surface without actually making hard contact. By adjusting height to maintain a set-point frequency the surface topography can be revealed [89]. By minimising the interaction forces, and hence area, between the probe and sample very high resolution images may be obtained even of soft sample, although the technique is more difficult to achieve than for other modes [90].

As well as imaging, by keeping the probe static in the *x* and *y* directions and scanning purely along the *z*-axis, interaction forces may be examined using this technique. For researchers interested in studying membranes, this feature of the AFM can be used to study foulant membrane interactions under a variety of operating conditions. This mode of operation has been reported in the literature for the study of adhesion forces [91-96], long range interaction forces [97-101], surface mechanical properties [91, 102-106] and the bond strengths of biomolecular interactions [107-109]. Raw force interaction profiles are obtained as deflection signal (in V or nA) versus piezo position. With calibration for the cantilever spring constant and the optical lever sensitivity, these raw values can

be converted to allow plots of interaction force versus probe sample separation. This process is covered in more detail elsewhere [110-112].

<insert figure 9 here>

An example force distance curve is shown in figure 9. The red trace shows the approach of the tip to the surface, and blue is the retract trace. Here repulsive forces are set as positive. At large separation distances net interaction forces are zero. As the tip approaches the surface long range interaction forces cause the cantilever to become deflected. As the tip contacts the surface a linear repulsive interaction causes the cantilever to be deflected upwards. On retraction this is reversed, with adhesive forces casing a hysteresis in the force profile prior to the tip becoming detached. The cantilever then returns to its free level.

To obtain information about interaction forces between materials of interest the sharp imaging tip can be chemically functionalised or replaced with a particle of the material of interest, or replaced with a microsphere functionalised with the material of interest. These latter two are commonly referred to as 'colloid probes' and are of interest for studying interactions between foulants and membrane surfaces. The use of colloid probes was first reported by Ducker *et al* [113] who used a silica microsphere to probe the effect of solution pH and ionic strength on interactions between silica and polystyrene surfaces. Measurement of long range interactions can give an estimate of the ability of a surface to reject attachment depending upon environmental conditions, whilst measurement of the adhesion force can demonstrate the strength of attachment of deposited foulants. Adhesion forces between a silica sphere and PES membranes were used to gauge the effect of 2-dimethyl-aminoethylmethacrylate (qDMAEMA) modification on fouling of membranes by silicates [114].

3.1.2 Membrane Surface Characterisation

If the surface pore diameters of a membrane are sufficiently large to visualise using AFM equipment then it is possible to obtain the mean pore-size and pore-size distribution. If a sufficient number of

pores have been measured then the following probability density function may be used to describe the pore size distribution [115, 116]:

$$\frac{df(d_p)}{d(d_{p)}} = \frac{1}{d_p \ln \sigma_p \sqrt{2\pi}} \; exp\left[-\frac{\left(\ln d_p - ln\, \mu_p\right)^2}{2\left(\ln \sigma_p\right)^2}\right] \qquad (3)$$

where d_p is pore size, μ_p is mean pore size and σ_p is the geometric standard deviation of the pore sizes. A log normal plot allows calculation of d_p and μ_p. Using a plot of the cumulative distribution, μ_p is the pore size found at 50 % of the cumulative total and σ_p is the ratio of pore sizes at 50 % and 84.13 % of the cumulative distribution [117].

In general it has been found that the pore sizes measured using this method show some divergence from those obtained from membrane transport methods or porosimetry [117, 118]. This is in large part due to AFM being a surface technique, and as such it only measures the pore opening size, whereas other techniques may give the critical pore size, which is the minimum pore size within the membrane material. In addition, pore size results reported potentially include sizes of openings in the surface which may not be propagated through the membrane, as well as image convolution effects which can become pronounced when features on a size-scale equivalent to the size of surface asperities are being examined. This latter issue has been addressed by using specialised probes with carbon nanotubes mounted to give a very sharp and high aspect ratio tip [119], which gives better resolution to nanofiltration pores.

Through the observation of changes to surface morphology and related quantitative parameters, such as roughness, AFM imaging is of utility for providing characterization information during the development and modification of membrane surfaces. For instance, Shirazi *et al* [88] used AFM to monitor effects of varying fabricate conditions of polystyrene hollow fibre membranes produced by electrospinning followed by contact heating. Vacuum oven heating decreased surface roughness and a more homogenous pore geometry. Skewness values became more positive with heat treatment, which could be related to the smaller pore size and thicker fibres seen in AFM and SEM images. Skewness is a roughness statistic which describes the shape of the height distribution of the

surface, with negative values representing a distribution with a tail for values lower than the mean, positive with a tail for values greater.

<insert figure 10 here>

AFM was utilized by Matin *et al* [120] to monitor morphological changes to the surfaces of commercial PA membranes after modification to reduce fouling. Changes to the roughness were negligible, which was attributed to a smooth, even film on the surface deposited by the chemical vapour deposition method. It is worth noting that all of the surface roughness parameters are just statistical descriptors of the height distribution of pixels in an image, which means it is possible to have radically different surface topographies and have identical values for a particular parameter. As a result, researchers should be careful not to rely on a single roughness parameter in isolation to describe surface changes. PVDF membranes were modified using high molecular weight poly-ethylene glycol (PEG) by Chang *et al* [72] who observed an increase in roughness as the degree of modification was increased when PEG overlayers were complete. As the overlayers became completed the roughness then began to decline with increasing degree of modification.

The effect of mode and environment on imaging of PES membranes of differing hydrophobicity were investigated by Johnson *et al* [71]. When using tapping mode in water for a moderately hydrophobic membrane, with a water contact angle of 72°, globular surface features were observed (figure 10). These features did not appear in images obtained from tapping mode in air, or contact mode in air or water for this membrane and were not observed at all on a hydrophilic membrane. Cross-sections of these features could all be fitted by the equation of a circle, demonstrating that they were spherical caps. It was suggested that these features may be small pockets of air adhering to the hydrophobic surface, or 'nanobubbles', previously observed on other hydrophobic surfaces [121-124].

<insert figure 11 here>

Kochkodan *et al* [125] used the layer by layer technique for modification of commercial PA nanofiltration membranes. Representative AFM scans are shown in figure 11, showing unmodified

NF-90 membrane and membranes modified with successive layers of poly-[(4-styrenesulfonic acid) co-(maleic acid)]. It was observed that the surface roughness reduced as the number of layers increased, likely due to filling in of valleys by deposited electrolyte layers. Kaner *et al* [126] also used a layer by layer approach to modify PES membranes with AgCl xerogels incorporated into chitosan in an attempt to produce low biofouling membranes. Membranes modified with single layers of chitosan alone had lower roughness than surfaces modified with chitosan layers incorporating the xerogels.

3.1.3 Investigation of Membrane Scaling

Scaling of membranes by inorganics is a major issue in membrane treatment of saline or brackish water, leading to extensive investigation of the process. Force distance measurements using a silica particle probe were used by Mi and Elimelech to investigate scaling of cellulose triacetate (CT) and PA forward osmosis membranes in the presence of dissolved silica [127]. In the absence of dissolved silica adhesion forces were greater for CT than PA, due to the CT membrane having a greater density of hydroxyl groups available for hydrogen bonds. When measurements were repeated in 4.2 mM dissolved silica, adhesion forces for both membranes increased markedly, with detachment events occurring away from the membrane surface. This was due to the formation for a silica gel between the probe and membrane surface.

The effect of dry-out on scaling of PVDF and PTFE membranes using simulated membrane distillation conditions were investigated by Guillen-Burrieza *et al* [128]. It was found that pristine PTFE membranes had much rougher surfaces than scaled membranes, whereas for PVDF membranes the opposite effect was observed. The radically different morphology of the two membranes was used to explain this. The rougher and more open structure of the PTFE membrane was filled in by deposited salt crystals leading to a reduction of roughness. However, salt crystals were seen to be

deposited on the surface of the PVDF membrane, leading to increased surface roughness. Forces measured between a $CaCO_3$ colloid probe and the membranes showed a greater adhesion force for the PVDF membrane than for PTFE. This was ascribed to the increased roughness of the PTFE membrane decreasing the area of interaction. Wetting behaviour was ruled out as an alternative explanation due to the two membranes having similar water contact angles, but contributions of chemical interactions couldn't be entirely excepted. Adhesion forces showed a good correlation with the degree of fouling during membrane distillation tests. This is likely to be due to a greater adhesion force demonstrating a more stable attachment of salt micro-crystals to the membrane surface and acting as nucleation sites for initiation of crystal growth.

3.1.4 Investigation of Organic and Biofouling of Membranes

Fouling of membranes by organic material is complex due to the wide variety of chemicals involved, which can include the breakdown products of plants, such as humic and fulvic substances, and also macromolecules such as proteins, fatty acids and polysaccharides produced by microorganisms (extra-cellular polymeric substances, EPS) and from waste discharge into the sea or freshwater. EPS is usually found alongside living microbial cells, so as such organic and biofouling often may occur simultaneously, with EPS performing an import role for bacterial attachment to surface [73, 129].

Johnson *et al* [130] studied organic fouling of nanofiltration membranes (both commercial and modified with polymeric bicontinuous emulsion [131]) using polystyrene microspheres which had been functionalised with humic acid (HA) in pure water and model textile dye wastewater (MTDW) [132] to assess potential fouling of these membranes in membrane bioreactor applications. Measurements taken in the two environments showed completely different performances in adhesion tests, due to surface modification of both probe and membranes by the MTDW, as shown by water contact angle and ATR-FTIR measurements [130]. In clean water more hydrophobic surfaces favoured larger adhesion forces, whereas after exposure to MTDW more hydrophilic surfaces favoured greater adhesion forces. It was confirmed that this was due to MTDW exposure

transforming the HA probe from hydrophobic in nature to hydrophilic. ATR-FTIR observations showed that the MTDW (a mixture of surfactants, textile dyes, salt and glucose) caused different chemical modifications to the membranes depending upon their fabrication conditions.

EPS fouling of reverse osmosis surfaces was investigated by Tansel *et al* using AFM [133]. Initially a sub-layer was observed which consisted of discrete molecular units. After less than a day of cross flow filtration using an EPS solution an over-layer was formed, which was soft and easily removed by AFM scanning. The effect of EPS on membrane surface morphology was studied by Su *et al* [134] for several membranes. EPS extracted from activated sludge were found to increase roughness of all membranes, with the initially smoothest membrane being the most severely affected. Bowen *et al* [135] used BSA silica microspheres as probes to measure adhesion forces. Both membranes examined showed greater adhesion than when using bare silica microspheres, showing that modification of silica by dissolved polypeptides and proteins, found in EPS, is likely to increase the severity of silicate fouling.

The first experiments to measure interaction forces using AFM between living cells and membranes were carried out by Bowen *et al* [136], who used both a *Saccharomyces cerevisiae* cell and a BSA coated microsphere as an analogue. Membrane biofouling is a complex process, but use of live cells to measure adhesion forces has a number of drawbacks, including use of a soft cell making calibration of optical lever sensitivity uncertain, as well as the soft cells undergoing compression in a difficult to predict manner, which could potentially change during the life cycle of the cell. As such much biofouling work using AFM has used functionalised colloidal probes as a stand in for actual cells. For instance, Herzberg *et al* [137] used a used a carboxylated latex probe to simulate bacterial interactions with a reverse osmosis membrane coated with EPS and the effect of $CaCO_3$ in the surrounding medium. For pristine membranes, only repulsive forces were measured, whether Ca^{2+} was present or not; fouled membranes showed an attractive jump-in at close approaches when Ca^{2+} was present, with the attraction ascribed to binding of Ca^{2+} to carboxylate groups on the surfaces of the probe and fouling layer. A carboxylated probe was also used by Bernstein *et al* [138] to

investigate adhesion forces with RO membranes modified by graft polymerisation. It was found that changing of the charge states of the membranes by adjusting the pH showed that interactions were dominated by electrostatic double layer forces.

Zaky *et al* [139] investigated the fouling of CA membranes by both live and dead cells and used several roughness parameters calculated from AFM scans to assess the nature of the fouling at several stages. Root mean squared (RMS) roughness and skewedness for membranes used to filter active and inactive cells for 4 hours were similar to that of pristine membrane. RMS roughness stayed low after 11h for inactive cells, but increased after 24h of filtration, but the skewedness of the height distribution remained low. For active cells after 11h, RMS also remained low but the skewedness was higher, suggesting a greater amount of asperities on the surface. RMS did increase after 24h, but with the skewedness returning to zero. The authors used the differences in the skewedness observed at 11h to suggest a difference in the structure of the fouling layer made by active and inactive cells.

Quantitative data obtained from AFM imaging has been used by several researchers to guide computer models of membrane fouling. For example Demneth *et al* [116] used surface morphological information obtained from AFM scans to feed into and evaluate thermodynamic models of adsorption behaviour for membranes fouled with proteins, polysaccharides and HA. Several roughness parameters obtained from AFM scans were used by Chen *et al* [140] to develop mathematical models of several membrane surfaces by soluble microbial products and compared with filtration test data. Wetting behaviour and surface charge alone were not able to predict fouling behaviour, and interaction energies differed from that predicted for surfaces with low roughness. It was found that short range effect on colloidal interactions due to surface roughness lead to a decreased energy barrier to attachment.

3.2 Scanning Electron Microscopy (SEM)

3.2.1 Introduction and Basic Principles

Scanning electron microscopy operates by scanning a focussed beam of electrons onto the sample surface. Secondary electrons emitted by the sample, backscattered electrons and X-rays are captured by the appropriate detector and then used to build up an image of the sample surface or other information.

Interactions between beam electrons and the samples can be elastic or inelastic. If the interaction is inelastic then secondary electrons (SE) are emitted with different energy from the incident electrons. Conversely if the interaction is elastic then the electrons are deflected and scattering takes place: any electrons which are deflected at an angle greater than 90° are termed back-scattered electrons (BSE) and can be collected by a specialised detector.

For standard SEM, electrons are generated by thermionic emission from a tungsten filament, or a solid-state crystal, such as lanthanum hexaboride (LaB_6). Tungsten is the most commonly used, due to low cost and high reliability, whereas solid state crystal emitters produce a higher output for a given current and longer lifetime [141]. For field emission SEMs (FESEM) a different type of electron source is used, a field emission gun (FEG) which works on field emission due to a potential gradient. The FEG is usually made of a tungsten filament with a sharp tip (~0.5 nm): this combined with low acceleration voltages allows better resolving power at high magnifications than standard SEM. In addition, the lower acceleration voltages reduces the charging of non-conducting samples, reducing the need for metal coating to some extent. The FESEM is divided into three types, depending upon the type of FEG used: cold field emission (CFE), thermal field emission (TFE) and Schottky emission [142]. CFE has emitters have a high brightness, but are prone to contamination due to gasses emitted from the sample, which need to be removed periodically by heating the tip to a high temperature periodically, a process referred to as flashing [143]. TFE occurs at a much higher temperature than CFE, reducing the problem of contamination, leading to a more stable electron source.

SE tend to be relatively low in energy, (< 50 eV), meaning that they can only escape the upper several nanometres from the sample surface. As a result, the SE signal is capable of giving an

accurate depiction of the sample surface topography. Image contrast is obtained by features on the sample surface obscuring some emitted SE. BSE tend to have higher energy than SE, and are deflected differently depending upon the atomic number of the elements in the sample surface, with higher atomic number elements deflecting a greater proportion of incident electrons back towards the detector. As a result, the BSE image will contain contrast based upon the elemental composition of the sample.

Interaction of incident electrons with the sample surface can cause the emission of X-ray photons. Detection of this X-ray signal can give important information about the elemental composition of the surface, using a technique called energy dispersive X-ray (EDX) spectroscopy, in addition to surface imaging using SE and BSE. EDX spectroscopy can detect elements with higher atomic number than boron (5). When primary electrons from the electron beam displace electrons from a lower atomic orbital, an electron from a higher orbital will replace it, losing energy in the process which is emitted as an X-ray photon. As each element has a characteristic X-ray spectrum, the detected spectra allows elemental analysis of the sample surface [142].

3.2.2 Investigation of Membrane Surfaces using SEM

SEM has been extensively used by membrane technologists due to the high quality and high resolution images which can be obtained of the membrane surface and cross-sections, and for having fast image acquisition times compared with AFM and relatively easy sample preparation as compared with TEM.

For example, Galiano *et al* [131] used a FESEM in characterising novel membranes prepared by adding a polymerizable bi-continuous microemulsion (PBM) overlayer onto a commercial PES ultrafiltration membrane scaffold. Surface scans and scans of cross-sections through the membrane were made, in SE detection mode, as shown in figure 12, which shows the typical structure seen for bicontinuous systems. The PBM structure is made up of polymer channels (white strips) and water channels (dark strips) randomly distributed across the membrane surface, with water channels

having widths of 30-50 nm. Whilst surface scans are useful for gaining knowledge of the surface topography, scans of cross sections are useful for gaining insight into the internal structure of the membrane. In this case, it was seen from cross-sections that the PBM coating was clearly visible and less than 1 µm thick. The channels were essentially elongated pores. Bromley *et al* [144] showed that pore geometry is influential on fouling resistance to pore blocking, with critical flux being higher for slotted pores over circular pores, due to the geometry allowing fluid to flow around particles trapped in pore openings. This could in part explain the resistance to fouling which was observed for these PBM membranes [131]. SEM images showed a decrease in 30% of fouling layer deposited on the surface of the PBM membrane compared with the PES membrane after filtration tests using aqueous HA solutions as feed-water. This result was in agreement with water permeability tests, which showed lower flux decline for the PBM membrane.

<Insert figure 12 here>

Wang *et al* [145] created nanocomposite membranes containing single walled and multi-walled carbon nanotubes (SWNT and MWNT respectively) in a PVDF matrix. SEM analysis demonstrated that CNTs formed granular aggregates, which formed a separate CNT layer on the top surface of the membrane. SWNT also were observed to form bundles. These CNT layers formed porous filtration layers, with pore sizes of >10 nm suggesting that size-exclusion mechanisms would be largely negligible or filtration of small molecules.

As mentioned above, BSE imaging is able to show contrast between different materials. For instance, Buonomenna *et al* [146] utilised this feature when studying PVDF membranes containing Ti(IV)/trialkanolamine complexes to create catalytic membranes. As can be seen in the cross-section shown in figure 13 a) these Ti-containing complexes show a sharp contrast (dark) with the lighter shaded surrounding membrane material. It can be seen that the Ti(IV)/trialkanolamine complexes are uniformly distributed throughout the membrane structure. EDX spectra were analysed at different depths in the cross-sectional image (figure 13 b) and showed the same spectra, all with a clearly visible Ti peak, confirming this uniformity. EDX surface scans of this membrane also showed

that the Ti was uniformly dispersed across the membrane surface at high density, and that the Ti was dispersed as fine particles rather than having re-crystallised into large particles.

<insert figure 13 here>

3.3 Transmission Electron Microscopy (TEM)

3.3.1 Introduction and Basic Principles of TEM

Unlike SEM, where secondary electrons emitted from the surface or backscattered electrons deflected by more than 90° are detected, transmission electron microscopy (TEM) deals with electrons which transmit directly through a sample of interest. As a result, samples are required to be extremely thin (~100 nm), and are often milled to get them thin enough, but extremely high resolutions can be achieved under suitable conditions, with almost atomic resolution possible.

A beam of high energy electrons is focussed by being passed through a series of electromagnetic lenses and metal apertures, it is then passed through the sample, which is mounted on a sample holder (TEM grid) from where they pass, after refocussing by further electromagnetic lenses, to a detector (usually a charge coupled device or CCD) [147]. The beam of electrons is affected by sample thickness, density and material composition. All measurements occur under vacuum. Sample preparation depends on the sample to be examined, and can include ion milling, focussed ion-beam (FIB), chemical etching, ultra-microtome, ball milling, mechanical polishing etc.

Two different types of image are produced by TEM – dark field and bright field images, produced by diffracted and transmitted electrons respectively [148]. For bright field images the image is due to directly transmitted electrons, so image contrast is as a result to attenuation of the beam with varying sample density. With dark field mode only diffracted electrons are received by the detector, therefore this mode can give information on crystal structure of the sample.

Image contrast in TEM is a result of the interactions between electrons in the incident beam with sample material. Electrons within the sample behave as a wave and interactions can cause both the amplitude and frequency of that wave to alter. The interactions may be due to several mechanisms:

thickness-mass contrast, diffraction contrast or phase contrast. For thickness-mass contrast, this is due to variations in thickness and or density of the sample changing the number of interactions with electrons which will occur. Diffraction contrast is due to diffraction of electrons, following Bragg's law. This can be affected by crystal structure and sample orientation. Phase contrast imaging allows high resolution images to be created by exploiting the phase contrast which arises from interference between transmitted and diffracted beams, if the detector is orientated to capture both [147]. As for SEM, X-rays emitted from the sample by interaction with beam electrons can be collected and analysed using EDX analysis.

Typically, to obtain cross sections of membranes suitable for TEM imaging, fabric or polymer (if present) is carefully removed before immersing the membrane in a suitable resin. Once set, slices of less than 100nm thickness are made through the resin block using an ultra-microtome [149, 150]. For imaging of the membrane plane milling techniques, as measured above, may be necessary. However, thin films thin enough for TEM measurements may be prepared by careful removal or dissolution of any backing layer, for example preparation of polyamide thin films from a PA / PSF composite membrane by dissolution of the PSF layer using chloroform, as described by Pacheco *et al* [151].

3.3.2 Characterization of Membranes using TEM

<insert figure 14 here>

TEM was used by Jeong *et al* [150] to study the *in situ* interfacial polymerization of nanocomposite thin films on PSF support layers. The created thin films consisted of zeolite nanoparticles embedded in a PA matrix. Figure 14 shows a TEM cross section image for pure polyamide thin film (a) and zeolite-polyamide thin film (b) on a PSF support layer. The high degree of observed roughness prevented accurate film thickness measurements, with thickness varying for both films in the range of 50 – 200 nm. Zeolite particles had a high contrast with the PA matrix, showing as dark particles within the film and at the interface. Al peaks in the EDX spectra confirmed the presence of zeolite at

these points. To examine the structure of polyamide films in isolation Pacheco *et al* [151] exposed TEM cross-sections of PA/PES composite membranes to chloroform, which dissolved the PSF layer. This was carried out due to difficulties discerning the PA and PSF interface: removing the PSF layer was carried out to make this clearer. The PA film was seen to consist of a nodular base of PA, from which a ridged structure projected on the opposite side to the PA/PSF interface, which was relatively smooth.

<insert figure 15 here>

Freger *et al* [149] also studied thin film composite PA membrane structures using TEM. The PA layers were modified with acrylic acid (AA) monomers. To improve contrast, samples were stained with uranyl ions, which readily attached to the AA monomers through ion-exchange with free carboxylic groups. PSF support appeared darker than the PA layer due to the S atoms present in PSF. It was seen that the grafted polymer layer was approximately 20 nm thick.

As well as 2-dimensional images through thin films, 3-dimensional imaging of the structure of thin films is possible using TEM tomography. For instance Pacheco *et al* [152] gained 3D structures of polyamide thin films in RO membranes, by tilting and re-imaging the sample at a large range of tilt angles (-70 to +70°). Software was then used to combine the large number of images into 3D reconstructions which could be visualised as static images or videos. In figure 15 is shown a representation of TEM images slicing through the sample surface to allow reconstruction of 3D structure. The tomograms obtained by the authors allowed visualisation of voids within the film and confirmed structural differences between RO membranes fabricated for use in brackish and saline water desalination, which explained the difference in the permeability of these membranes. The seawater RO membrane contained fewer voids and polyamide sections were thicker. It was suggested that the differences in permeability of these membranes was due to different pathways available to water molecules, with water passing through a void open to the backside of the film needing to cross fewer PA sections.

4 Measurement of Contact Angles of Membranes

4.1 Introduction and Basic Principles

Surface wetting is a phenomena which governs much of the interactions between fluids and solid surfaces, and as a result is of primary importance when considering membrane processes and plays a major role in defining flux rate, permeate rejection and surface fouling [153]. The degree of wetting is determined by the material properties of the membrane surface which govern interaction with water molecules, and are influenced by the liquid pH, temperature, charge density on the membrane surface and the interfacial interaction energy [154]. The degree of wettability, or hydrophobicity, can be determined from the contact angle formed by a droplet of fluid, most typically water, on the surface of interest.

<insert figure 16>

When considering a droplet on a flat surface, the contact angle, ϑ_c, is the inside angle between the tangent line, formed starting at the three-phase contact line and following the outside edge of the droplet, and the flat surface (figure 16). If the droplet tries to minimise the interaction area with the surface, then the contact angle must necessarily increase as the droplet takes on a shape closer to spherical. If the interaction between the droplet and surface is favourable and the surface becomes fully wetted, then the contact angle will approach zero. It then follows that, when using water droplets, the contact angle is a measure of the hydrophobicity of the surface, with contact angles approaching zero for hydrophilic surfaces and increasing to 90° for hydrophobic surfaces. Surfaces with water contact angle greater than 90° are often labelled as “super-hydrophobic”.

More specifically, the contact angle depends on the relative magnitudes of the interfacial tensions at the three interfaces involved (solid-liquid, solid-gas and liquid-gas), as described by the Young equation [155, 156]:

$$\cos\theta_c = \frac{\gamma_{SG} - \gamma_{SL}}{\gamma_{LG}} \qquad (4)$$

where γ_{SG}, γ_{SL} and γ_{LG} are the interfacial tensions for the solid-gas, solid-liquid and liquid-gas boundaries respectively (see figure 16). Line tension, that is a one-dimensional tension along the three-phase contact line, also contributes, but for macroscopic measurements is insignificant and disregarded. However, due to scaling effects this becomes significant when considering contact angles on a microscopic scale [157].

The Young equation assumes an idealised surface, i.e. one which is smooth, chemically inert, homogenous, non-porous and insoluble, a list which most surfaces violate in one way or another [158, 159]. Deviation from this ideal behaviour leads to different contact angle values to those predicted, and surface roughness and inhomogeneity can lead to different values obtained from different parts of the surface.

One particular phenomenon arising from this non-ideal behaviour is that of contact angle hysteresis. The Young equation describes a 'static' contact angle, where the energy balance between the three interfaces are in equilibrium. For a surface with heterogeneities, different contact angle values may be obtained when the droplet is advancing across a surface (ϑ_a) or is receding (ϑ_r), with the difference between the values termed the contact angle hysteresis, *H* [160, 161]:

$$H = \theta_a - \theta_r \qquad (5)$$

For a moving droplet, either rolling on a slope or moving due to a change in quantity of liquid in that droplet (due to, for instance, evaporation or condensation) the advancing edge of that droplet is pinned until the advancing contact angle is reached; a receding droplet edge does not move until the receding contact angle is reached. The static contact angle is a metastable position which can have any value between ϑ_a or ϑ_r [162]. As a result, for surfaces with significant *H*, the static contact angle may not be very useful. For more comprehensive information on this phenomenon please see the following references: [160, 161, 163].

Wenzel studied the effect of roughness on the static contact angles measured for a homogenous surface [164]. He considered the contribution of a roughness factor, *r*, which is the ratio of the actual surface area to the planar projection of the same area. The Wenzel equation was derived assuming that the droplet is in continuous contact with the sample surface, with the water penetrating fully into any crevices [156]:

$$\cos\theta_w = r\,cos\theta_c \qquad (6)$$

where ϑw is the Wenzel contact angle. This equation does not take into account sizes of surface features or their geometry.

The Cassie-Baxter equation also derives static contact angles for surfaces with roughness but, unlike the Wenzel equation, was derived for the case where the droplet does not penetrate surface crevices, instead sitting atop a rough surface with surface crevices filled with gas in between the droplet and surface [165]:

$$cos\theta_C = f_1\,cos\theta_1 - f_2 \qquad (7)$$

where ϑ_1 is the contact angle for a smooth surface of the same material and f_1 and f_2, are the fractions of the surface covered by the solid liquid and liquid air interfaces respectively ($f_1 + f_2 = 1$) [166, 167].

4.2 Techniques for Measuring Contact angles

The sessile drop method for measuring surface contact angle is perhaps the simplest and most widely reported. It essentially consists of a single drop of liquid placed on a level sample surface. Contact angle is determined by direct viewing. Modern systems incorporate capture of the droplet image digitally, which is then processed on a computer to calculate the contact angle directly from the image. This technique is simple in operation, with fast processing of results, with small sample and droplet sizes required. Figure 17 shows an example of a droplet placed on a surface for contact angle measurement using this technique.

<insert figure 17 here>

Measurement of static contact angles is as straightforward as described above. To measure advancing and receding contact angles several approaches are possible. Firstly, the needle producing the droplet may be used to add or remove more water to or from the droplet, allowing advancing and receding angles to be measured respectively. Ideally the needle should be as small as possible relative to the droplet to minimise any inaccuracies due to the presence of the needle distorting the shape of the droplet. Secondly, a tilting platform may be used. This will allow measurement of the advancing and receding contact angles simultaneously from the downslope and upslope parts of the droplet – these angles are the angles at which the respective contact lines will become unpinned from the surface, allowing the drops to move. Thirdly, material can be removed from the droplet by evaporation in a dry atmosphere leading to the receding contact angle becoming apparent, or increased by condensation in a humid atmosphere, allowing advancing contact angle to be measured.

It should also be noted that the measured contact angle of membranes may vary depending whether they are in a hydrated or dehydrated state. In addition, for a porous hydrophilic membrane in a dehydrated state, small droplets are liable to penetrate the membrane surface rapidly, making obtaining a stable droplet difficult.

One other issue which should be noted is the effect of drop size on measured contact angles. Drelich reviewed the literature [168] and found that whilst the advancing contact angle was only slightly affected by the drop size, receding contact angle measurements changed significantly from droplets with a base diameter of less than 5-7mm, making comparison of measurements between different laboratories problematic.

Alternatively, a bubble of air can be introduced to the surface of a sample immersed in water. The sample is generally inverted, with the bubble placed below the membrane to keep the bubble in contact with the surface in order to overcome the issue of the bubble detaching if its buoyancy is sufficient to overcome its attachment to the surface. Here the set-up is the inverse as that measured

using the sessile drop procedure, with the external angle of the bubble giving the water contact angle, rather than the internal angle. Zhang *et al* [169] compared the sessile drop and captive bubble methods for measuring contact angles on ultrafiltration membranes. In most cases the results from the two methods were in good agreement, with differences within statistically expected ranges. However, one membrane did show a significant difference for measured advancing contact angle. It was noted that this particular membrane showed a time dependant change in the measured receding contact angle and the authors offered a possible explanation as being that this particular membrane changes its surface structure more easily than the other membranes, thereby adapting to the surrounding medium leading to a change in surface energy.

Another method to obtain contact angle measurements is by the Wilhelmy plate method. Here a smooth and thin plate of a material of interest is lowered edge-first into a liquid of known surface tension. If the contact angle between the plate and the liquid at the meniscus is < 90°, then a measurable downward force is exerted, as given by the following relationship [170]:

$$W_f = p\,\gamma_{LV}\,cos\theta_c - V\Delta\rho g \qquad (8)$$

where W_f is the measured downward force, p is the perimeter of the three-phase contact, V is the volume of liquid displaced by the plate, $\Delta\rho$ is the density difference between liquid and vapour and g is the acceleration due to gravity. Advancing and receding contact angles can be calculated by moving the plate up and down through the liquid surface [170]. The sample needs to be flat and rectangular, to have regular geometry, and have identical characteristics in all planes. As such this technique is not likely to be useful for asymmetric membranes.

Contact angle can also be measured from observing the capillary rise between two closely spaced vertical plates dipped into a liquid of known surface tension. The following relationship, derived from the Young-Laplace equation, can then be used to calculate the contact angle [171]:

$$h = \frac{2\gamma_{LV}\, cos\theta}{\Delta\rho\; g\; w} \qquad (9)$$

where *h* is the rise height of the capillary front and *w* is the separation distance between the two plates.

4.3 Contact Angle Measurements of Membrane Surfaces

The wetting of membranes is of fundamental importance in their performance, affecting water flux, solute rejection and playing a large role in their fouling behaviour, as these properties depend on chemical interactions at the interface between the feed water and the membrane surface. The majority of commercially available membranes are made from hydrophobic polymers, selected for their chemical, mechanical and thermal stability [172]. Fouling of membranes by organic and microbial substances is well known to be less severe for hydrophilic surfaces compared with hydrophobic [173]. As such, much work on the performance improvement of membranes by surface modification has concentrated on adjusting their hydrophobicity. In this section we will endeavour to give a few examples from the literature where water contact angle measurements are used to determine properties of water filtration membranes. This is not intended to be an exhaustive review, as the literature is extensive. We would instead direct the reader to the recent review by Hebbar *et al* [174].

Garcia-Payo *et al* investigated wettability of hydrophobic membranes, using contact angle analysis for pure water and aqueous solutions of alcohols to complement liquid entry pressure tests [175]. The authors noted that when distilled water was used the contact angle measurements were independent of pore size. It was also noted that the roughness of the membrane surfaces increased the contact angle from what was expected when compared with literature values for smooth surfaces of the sample materials.

<insert figure 18 here>

Membranes may be fabricated *de novo* to be hydrophilic, by selection of the appropriate polymers, or may be further modified after fabrication to increase the surface hydrophilicity – this may be to laboratory fabricated membranes or to commercially available membranes. There are a wide variety of modification techniques currently used: interfacial polymerization; surface grafting, including photo-initiated grafting and plasma induced grafting; chemical vapour deposition; surface coating; and incorporation of nano-fillers into membrane surfaces to name several.

PES / terpolymer blended membranes were fabricated by Li *et al* [176] using poly (acrylonitrile-acrylic acid acid-vinyl pyrrolidone). It was observed that there was a correlation between the proportion of the terpolymer incorporated into the membrane and the surface hydrophilicity. The change in water contact angle was ascribed to the acrylic acid and vinyl pyrrolidone chains on the membrane surface. The effect of hydrophilicity on membrane fouling due to protein was studied by Chen et al, who incorporated poly ethylene oxide (PEO) into poly acrylonitryl (PAN) ultrafiltration membranes [177]. This was carried out using PAN-graft-PEO copolymers using an immersion precipitation phase inversion method. The enrichment of the surface with PEO lead to a great reduction in the water contact angle (see figure 18) values measured, with higher concentrations of PEO at the surface having the greatest reduction. The effect of surface modification on flux decline whilst filtering aqueous solutions of bovine serum albumin (BSA) was studied, with the unmodified PAN membrane having the greatest flux decline. For membranes with contact angles of over 50° significant flux decline was observed, but flux decline was significantly retarded for the membranes with lower contact angles. Static adsorption of BSA was shown to be lowest for these two membranes also. For suspensions of *E. coli* bacteria and humic acid a similar behaviour was observed with the more hydrophilic membranes having lowest flux loss.

PSF membranes incorporating the hydrophilic polysaccharide chitosan alongside TiO_2 nanotubes were prepared by Kumar *et al* [178]. Water contact measurements using the sessile drop technique showed a drop in contact angle compared with the unmodified membrane. All the modified membranes showed a higher fouling resistance and flux recovery than the nascent unmodified

membrane as measured during filtration tests with BSA solutions. The fouling resistance of PSF membranes was improved by using N-succinyl-chitosan (NSCS) as an additive during membrane fabrication [179]. The hydrophilic NSCS decreased the water contact angle of the membranes, which correlated with the reduction of membrane fouling by BSA.

Khayet and Matsuura prepared polyetherimide membranes containing a fluorinated surface modifying macromolecule (SMM) using the phase inversion method [180]. Addition of the SMM made the surface more hydrophobic, as shown by water contact angle measurements. This was seen to correlate with an increase in liquid entry pressure into dried membranes.

<insert figure 19 here>

Al-Amoudi *et al* [181] used contact angle measurements to assess effects of fouling and cleaning on the surface properties of a variety of membranes. The membranes were all commercial membranes containing a top active layer composed of polypiperazinamide. Fouled membrane samples were obtained during membrane autopsy of one of these membranes after operating in a commercial seawater RO plant. The fouled membrane had a contact angle which was over 20° higher than for pristine membrane, suggesting organic fouling had occurred. Cleaning treatments using HCl and NaOH solutions reduced the contact angle of the fouled membranes, but they did not return to the unfouled value. Treatment with sodium dodecyl sulfate (SDS) greatly reduced the contact angle of both pristine and fouled membranes to 28° and 25° respectively. An inverse correlation was also noted between the contact angle for the membranes and the pure water flux for both virgin and fouled membranes (see figure 19).

5. Characterisation of Membrane Surface Charge

5.1 Introduction and Basic Principles

Polymeric and ceramic filtration membranes typically will carry ionizable features at the surface, or even ionic species in the case of ion-exchange membranes. As a result, in aqueous solutions the surface will carry a charge, the sign and magnitude of which depends on the environmental pH and

ionic concentration. Feed solutions are typically complex mixtures containing a wide variety of charge carrying substances including surfactants, macromolecules (e.g. proteins, polysaccharides, and nucleic acids), ions, polyelectrolytes. Interactions between these species and the membrane surface can significantly alter the surface charge of the membrane. Due to the charge interactions between the membrane surface and charged solutes and particulates, the charge of the membrane surface plays a significant role in mediating the separation properties of the membrane, the nature and extent of fouling and also concentration polarization. As such it is of great interest to people working with separation membranes to be able to determine the surface charge of the membrane under a range of different conditions.

The arrangement of charged species in close proximity to the membrane surface is referred to as the electrical double layer (EDL) [182]. Charge distribution in the EDL is most concentrated in close proximity to the membrane and decreases with increasing distance from the membrane (as illustrated in figure 20) reflected by a steady decrease in potential [183, 184]. Ions close to the membrane surface are in the immobile Stern layer. The Stern layer may be further sub-divided into the inner Helmholtz layer, contained between the membrane surface and the inner Helmholtz plane, which consists of partially dehydrated ions bonded to the surface chemically or electrostatically, and the outer Helmholtz layer found between the inner and outer Helmholtz planes, consisting of hydrated ions of typically opposite charge to the inner Helmholtz ions. In the Stern layer the distribution of charge and electrical potential are determined by geometrical constraints and interactions between ions, dipoles and the membrane surface. Beyond the Stern layer and separated from it by the shear plane, is the diffuse Gouey-Chapman layer where ions are free to move by thermally driven motion.

Actual membrane surface potential is very difficult to measure directly. Estimation of the zeta- (ζ) potential at the shear, or slip, plane is more accessible, leading to its extensive use when studying the electrical potential of membranes.

<insert figure 20>

There are a number of electrokinetic methods available. The primary ones of interest to researchers studying membrane phenomenon are electrophoresis, electro-osmosis, sedimentation potential and streaming potential. For electrophoresis and electro-osmosis an electrical field is applied to cause motion in the solid or liquid phase, whereas streaming potential and sedimentation potential measure a change in electrical potential due to movement of the solid or liquid phase. Electrophoresis and sedimentation potential both study the motion of a solid phase in a stationary liquid phase, which makes them suitable for study of the electrostatic behaviour of suspended particulates. Streaming potential and electro-osmosis both have a stationary solid phase and mobile liquid phase, making them more suited to the study of the electrical potential of membrane surfaces. There are a number of other electrokinetic phenomena which have been used to probe the electrical potential of surfaces in electrolyte solutions, including dielectric dispersion, streaming current, colloid vibration potential, electrokinetic sonic amplitude and surface conduction [185].

5.2 Techniques to Measure Membrane Surface Potential

5.2.1 Streaming Potential Measurement

When a fluid containing charged ionic species is allowed to flow through a charged membrane, capillary, plug or diaphragm due to a pressure gradient then the potential difference measured at zero current is the streaming potential [16]. The streaming potential is dependent upon a number of solution properties including the ζ-potential, solution viscosity, ionic diffusivities and dielectric constant.

For measurements the streaming potential can be generated in two ways. The electrolyte solution can be forced through a porous material, such as membrane pores, to measure the transverse

streaming potential. Here the electrical double layer in the pores is being measured, with errors arising if an overlap in the double layer from opposite sides of the pores occurs. Secondly the electrolyte can be forced through a narrow channel formed by the membrane being sandwiched between two plates, with the flow across the surface of the membrane, allowing measurement of the tangential streaming potential.

<insert figure 21>

When electrolyte solutions are pumped through a porous material, a capillary or through any narrow channel, a streaming potential is generated (see figure 21). The solution within the pore or channel carries a net charge (fig. 21a), so when it flows it generates a streaming current, I_S (fig. 21b), which gives rise to a potential difference, ΔE (fig 21c), which in turn opposes the movement of ions. This is because as counter-charges accumulate downstream the streaming potential arises which leads to a conduction current in the reverse direction (leading to back diffusion by ion diffusion and electro-osmotic flow), termed the leak current, I_L (fig.21d) [183, 186]. At equilibrium, the leak current and streaming current are equal in magnitude. The measured potential difference across the membrane or capillary at this point is the streaming potential. The ζ-potential is related to the streaming potential and applied pressure difference by [182, 187, 188]:

$$\zeta = \frac{\Delta E_{str}}{\varepsilon_r \, \Delta P} \; \eta \left(\lambda_0 + \frac{2\lambda_s}{r} \right) \qquad (9)$$

where ΔE_{str} is the streaming potential, ε_r is the relative permittivity of the medium, ΔP is the applied pressure, λ_0 and λ_s are the bulk and surface conductivity respectively, η is solution viscosity, and r is the radius of pore or capillary or half the width of a slit.

Experimentally the voltage difference across or along the membrane (ΔE) is determined at a range of flow rates. Assuming the conductivity of the membrane is lower than that of the electrolyte, a plot of ΔE versus ΔP should be linear, allowing the ζ-potential to be calculated from the gradient using the classic formulation of the Helmholtz-Smoluchowski equation [184]:

$$\zeta = \frac{\Delta E}{\Delta P} \frac{\eta}{\varepsilon_r \varepsilon_0} K_B \qquad (10)$$

where K_B is the specific conductivity of the electrolyte solution and ε_0 is the permittivity of vacuum. However, there are some limitations. The liquid flow through membrane pores or capillary needs to be laminar with the capillary radius greater than the Debye length (*1/κ*, the characteristic width of the double layer) as well as the surface having an electrical potential less than approximately 25 mV [184]. Also, linearity of *ΔE/ΔP* is not preserved at very low salt concentrations, and at high salt concentrations *ΔE* values are very low and sensitive, limiting the range of salt concentrations suitable for streaming potential measurements [189]. In addition, equation 10 is only applicable when the membrane surface conductivity is lower than the electrolyte, otherwise, for instance at low electrolyte concentrations, equation 9 is preferable. This requires knowledge of the membrane surface conductivity, which can be difficult to measure and is usually resolved by measurements of resistance of the electrolyte solution in the pore and comparing with measurements at high salt concentrations where surface conductivity is nullified [184, 190, 191]. It should also be noted that the Helmholtz-Schmolukovski equation is a simplified description of double layer behaviour. A complete solution would require solving the Nernst-Planck equation for ionic transport [192], although in most cases eq.s 9 and 10 are adequate.

During transverse streaming potential measurements, electrolyte flow through membrane pores allows determination of ζ-potential. In this case the membrane is placed between two electrodes to allow voltage across the membrane to be directly measured. This technique is relatively simple to carry out, but does have a number of limitations, restricting its utility. Firstly, for membranes consisting of multiple layers, each layer will contribute to the measured ζ-potential value, rather than just the ζ-potential of the uppermost layer, which is the one of most interest. In addition, this is also unsuitable for membranes with small pore sizes. This is because when the pore diameter is below the Debye length (double layer thickness), overlap of the double layer from opposite sides of

the pore occur. This invalidates the Helmholtz-Schmolukovski equation which is not valid for overlapping double layers [193, 194]. For microfiltration membranes this is unlikely to be a problem, but for tighter membranes the tangential streaming potential method is likely to be more reliable.

For tangential streaming potential measurements, electrolyte flow is along the membrane surface, rather than through the membrane pores. A flow channel is typically constructed, with the channel formed by two identical membrane surfaces facing each other with a narrow separation distance. Tangential measurements overcome several deficiencies in the transverse streaming potential technique. A primary advantage is that the channel width is set by the instrument not the material, so there is no problem with invalidating the Helmholtz-Schmolukovski equation due to overlapping double-layers - this also allows materials with very small pores to be measured and also removes problems due to high pressure drop and rejection of ionic species by such membranes. As flow is along the membrane surface and not though the material, contribution of pores, multilayers etc. are ignored and only the ζ-potential of the uppermost part of the membrane surface is measured. As such this technique is much more commonly used compared with transverse streaming potential measurements to measure the ζ-potential of polymer membranes.

Early work using tangential streaming potential measurements by Elimelech *et al* [186] studied the effect of solution pH, ionic strength and presence of humic acid on the surface charge of several commercial RO membranes. They concluded that as well as confirming this technique as being effective for ζ-potential measurement of RO membranes, that the cellulose acetate and polyamide membranes were negatively charged at all conditions, becoming more negative with increase pH and salt concentration and that the surface charge were significantly influenced by adsorption of humic substances and chemical substances introduced during membrane synthesis.

5.2.2 Electro-Osmosis

When an electrical current is applied across a porous membrane, plug or capillary filled with an electrolyte solution then a flow of material will occur. Observation of the subsequent flow velocity

when compared with the applied current will give some information about the surface charge or potential. The following equation for large pores at high ionic strength can be used to calculate the ζ-potential during electro-osmosis measurements [195]:

$$\zeta = \frac{J_V \, 4\pi\eta k_0}{I_c \, \varepsilon_r} \qquad (11)$$

where J_V is the flow rate of the electrolyte solution, and I_C is the applied current. Several authors [196-198] have reported that higher values are obtained from electro-osmosis than for streaming potential measurements, particularly at low solution pH values, although this may be due to the shear plane being affected by the method used.

5.2.3 Sedimentation potential

Sedimentation potential is the potential generated when charged particles settle due to the force of gravity [185]. There is also a centrifugation potential, where sedimentation occurs in a centrifuge, rather than due to gravity. Charged particles set up an electrical field which is of identical sign in the direction of sedimentation, with a steady state being achieved by flow in the opposite directions of ions of the opposite charge.

5.2.4 Electrophoresis

Another major source of information on the electrical potential of surfaces is electrophoresis. During electrophoresis the liquid phase is static, whilst the solid phase, suspended in the electrolyte, moves. As such electrophoretic techniques are widely used, probably more than any other electro-kinetic technique, for the determination for particle surface ζ-potential and also for the separation of particles and molecules based on surface charge.

Typically, particles are introduced to a tank of electrolyte solution with oppositely charge electrodes at each end. Particles will migrate to oppositely charged electrodes at a velocity proportional to the

applied electric field and the surface ζ-potential. The ζ-potential can then be calculated using Henry's equation:

$$\zeta = \frac{3}{2}\frac{U\eta}{\varepsilon_0\varepsilon_r}\frac{1}{f_{(\kappa^{-1}a)}} \qquad (12)$$

where *U* is the proportionality constant, which is the ration of the measured particle velocity the applied electric field strength, and $f_{(\kappa^{-1}a)}$ is Henry's function, with *a* the particle diameter. For low values of $\kappa^{-1}a$ Henry's function can be disregarded; for high values the Smoluckovski approximation can be made:

$$\zeta = \frac{U\eta}{\varepsilon_0\varepsilon_r} \qquad (13)$$

The velocity of the charged particles is usually measured by the laser Doppler technique, which is based on observation of light scattering [193]. Measurement of intact membrane surfaces due to the mobile solid phase has mostly been reported to measure electrokinetic properties of fragments of ceramic [193, 199, 200], polymer [201] and metal oxide [202] membranes. Wang and Ku [202] compared measurements of TiO_2 membranes from tangential streaming potential measurements, with electro-phoretic measurements of TiO_2 particles. It was observed that the ζ-potential measurements gave very different values, but both had identical iso-electric points.

Thomas *et al* [203] used a novel laser Doppler electrophoresis combined with an electro-osmosis surface mapping based technique to directly measure the surface charge of polymer filtration membranes. This technique examined electrophoretic mobility of polystyrene tracer microparticles suspended in the electrolyte solution. Comparisons of the technique with tangential streaming potential were made. It was found that the novel technique gave identical results to streaming potential. Data acquisition was more laborious and required a larger number of sample preparation steps. However, only very small membrane samples were needed and the equipment is less expensive and can be used for particle sizing and ζ-potential measurement in addition to measuring membrane surface charge.

<Insert Table 1 here>

6.0 Conclusions

We have reviewed a number of experimental techniques and instruments of interest to membrane scientists studying surface properties and development of membranes. We have used a number of examples from the literature to illustrate the uses of each technique and the types of information they can generate which would be of interest to investigators intending to study the characteristics of membrane surfaces. In table 1 is presented a summary of these techniques, including advantages and disadvantages, to aid in selecting which techniques are most suitable in approaching a given characterisation task. However, it must be remembered that these techniques are never used in isolation. For most of the papers referred to in this review which describe characterisation of membrane surfaces, it is always more than one, and sometimes a battery of techniques, which are used to determine surface properties, with each of the techniques described here being complementary, having a useful part to bring to a whole understanding of the membrane surface and the interactions it will have with its environment.

The field of membrane characterisation is constantly changing and growing. Whilst some of the techniques and concepts described here are old and have been used as part of membrane development and studies for decades, techniques are being constantly refined and updated and new ways to apply them are constantly being developed. It is hoped that this review gives a good account of the major techniques available to membrane technologists as they exist at the current moment. In the years to come such techniques will undergo further refinement, improvement and development, and techniques and instruments as yet unthought of will one day be added to the arsenal.

ACKNOWLEDGMENT

The author would like to thank the Royal Society for funding this work through Royal Society International Collaboration Award (IC160133).

List of abbreviations

FTIR - Fourier Transform Infra-red Spectroscopy

ATR-FTIR - Attenuated Total Reflectance- Fourier Transform Infra-red Spectroscopy

NMR - Nuclear Magnetic Resonance

XPS - X-ray photon spectroscopy

EDX - Energy dispersive X-ray

SAXS - Small angle X-ray scattering

SANS - Small angle neutron scattering

ESR - Electron spin resonance

DRIFTS - Diffuse reflective spectroscopy

PVDF - poly(vinylidene fluoride)

ATRP - atom transfer radical polymerization

PNIPAAm - poly(N-isopropylacrylamide)

TERS - tip-enhanced Raman spectroscopy

SERS - surface-enhanced Raman spectroscopy

VIPS - surface-enhanced Raman spectroscopy

PEI - poly (ether-imide)

NMP - N- methyl pyrrolidone

PVP - polyvinylpyrrolidone

PP - polypropylene

CA - cellulose acetate

PPO - poly(2,6-dimethyl-1,4-phenylene oxide)

TEMPO - 2,2,6,6-tera-methyl-1-piperidinyloxy

PES - poly ether sulfone

PSF - poly sulfone

D - pore diameter

σ_{SL} - liquid-solid interfacial energy

T_m - bulk melting point

ΔH_f - bulk enthalpy of fusion

ρ_S - density of the crystalline solid

PSD - pore size distribution

PPO - polyphenylene oxide

RO - reverse osmosis

BSA - bovine serum albumin

HEL - hen egg lysozyme

MWCO - molecular weight cut-off

SWNT - single walled nanotubes

TFN - thin film nano-composite

PVA - poly (vinyl alcohol)

NF - nanofiltration

qDMAEMA - 2-dimethyl-aminoethylmethacrylate

d_p - individual pore size

μ_p - mean pore size

σ_p - geometric standard deviation of pore size

PEG - poly-ethylene glycol

CT - cellulose triacetate

PTFE - poly tetra-fluoro ethylene

EPS - extra-cellular polymeric substances

HA - humic acid

MTDW - model textile dye wastewater

RMS - root mean squared

SE - secondary electrons

FESEM - field emission scanning electron microscopy

FEG - field emission gun

CFE - cold field emission

TFE - thermal field emission

BSE - back scattered electrons

PBM - polymerizable bi-continuous microemulsion

MWCNT - multi-walled carbon nanotube

AA - acrylic acid

Θ	-	contact angle
γ	-	interfacial tension
W_f	-	downward force on Wilhelmy plate
V	-	displaced volume
P	-	density
w	-	separation distance between two plates
g	-	acceleration due to gravity
PEO	-	poly ethylene oxide
PAN	-	poly acrylonitryl
SMM	-	surface modifying macromolecule
SDS	-	sodium dodecyl sulfate
EDL	-	electrical double layer
ΔE	-	electrical potential
ΔP	-	pressure difference
η	-	solution viscosity
K_B	-	specific conductivity of electrolyte solution
κ	-	Debye length
J_V	-	Electolyte solution flow rate
I_C	-	Applied current
U	-	proportionality constant for electrophoresis
$f(k^{-1}a)$	-	Henry's function
ε_0	-	permittivity of vacuum
ε_r	-	dielectric constant

7.0 References

[1] P.R. Griffiths, J.A. De Haseth, Fourier transform infrared spectrometry, John Wiley & Sons, 2007.
[2] B.C. Smith, Fundamentals of Fourier transform infrared spectroscopy, CRC press, 2011.
[3] H. Abdul Mannan, H. Mukhtar, M. Shima Shaharun, M. Roslee Othman, T. Murugesan, Polysulfone/poly (ether sulfone) blended membranes for CO2 separation, Journal of Applied Polymer Science, 133 (2016).
[4] I. Moideen K, A.M. Isloor, A. Ismail, A. Obaid, H.-K. Fun, Fabrication and characterization of new PSF/PPSU UF blend membrane for heavy metal rejection, Desalination and Water Treatment, (2015) 1-10.
[5] H. Matsuyama, A. Terada, T. Nakagawara, Y. Kitamura, M. Teramoto, Facilitated transport of CO 2 through polyethylenimine/poly (vinyl alcohol) blend membrane, Journal of membrane science, 163 (1999) 221-227.
[6] N. Ochoa, M. Masuelli, J. Marchese, Effect of hydrophilicity on fouling of an emulsified oil wastewater with PVDF/PMMA membranes, Journal of membrane science, 226 (2003) 203-211.
[7] A. Gören, C. Costa, M.T. Machiavello, D. Cíntora-Juárez, J. Nunes-Pereira, J. Tirado, M.M. Silva, J.G. Ribelles, S. Lanceros-Méndez, Effect of the degree of porosity on the performance of poly (vinylidene fluoride-trifluoroethylene)/poly (ethylene oxide) blend membranes for lithium-ion battery separators, Solid State Ionics, 280 (2015) 1-9.
[8] E. Vakili, M.A. Semsarzadeh, B. Ghalei, M. Khoshbin, H. Nasiri, Characterization and Gas Permeation Properties of Synthesized Polyurethane-Polydimethylsiloxane/Polyamide 12-b-Polytetramethylene Glycol Blend Membranes, Silicon, 8 (2016) 75-85.
[9] A. Bottino, G. Capannelli, O. Monticelli, P. Piaggio, Poly (vinylidene fluoride) with improved functionalization for membrane production, Journal of membrane science, 166 (2000) 23-29.
[10] Z. Xu, L. Wan, X. Huang, Functionalization Methods for Membrane Surfaces, Surface Engineering of Polymer Membranes, (2009) 64-79.
[11] N. Saxena, C. Prabhavathy, S. De, S. DasGupta, Flux enhancement by argon–oxygen plasma treatment of polyethersulfone membranes, Separation and Purification Technology, 70 (2009) 160-165.
[12] B. Bae, B.-H. Chun, D. Kim, Surface characterization of microporous polypropylene membranes modified by plasma treatment, Polymer, 42 (2001) 7879-7885.
[13] D.S. Wavhal, E.R. Fisher, Hydrophilic modification of polyethersulfone membranes by low temperature plasma-induced graft polymerization, Journal of membrane science, 209 (2002) 255-269.
[14] J. Garcia-Ivars, M.-I. Iborra-Clar, M.-I. Alcaina-Miranda, J.-A. Mendoza-Roca, L. Pastor-Alcañiz, Surface photomodification of flat-sheet PES membranes with improved antifouling properties by varying UV irradiation time and additive solution pH, Chemical Engineering Journal, 283 (2016) 231-242.
[15] H. Liu, P.V. Gurgel, R.G. Carbonell, Preparation and characterization of anion exchange adsorptive nonwoven membranes with high protein binding capacity, Journal of membrane science, 493 (2015) 349-359.
[16] N. Singh, S.M. Husson, B. Zdyrko, I. Luzinov, Surface modification of microporous PVDF membranes by ATRP, Journal of membrane science, 262 (2005) 81-90.
[17] G. Zhao, W.-N. Chen, Enhanced PVDF membrane performance via surface modification by functional polymer poly (N-isopropylacrylamide) to control protein adsorption and bacterial adhesion, Reactive and Functional Polymers, 97 (2015) 19-29.
[18] S. Te Poele, J. Van der Graaf, Enzymatic cleaning in ultrafiltration of wastewater treatment plant effluent, Desalination, 179 (2005) 73-81.

[19] I. Donelli, P. Taddei, P.F. Smet, D. Poelman, V.A. Nierstrasz, G. Freddi, Enzymatic surface modification and functionalization of PET: a water contact angle, FTIR, and fluorescence spectroscopy study, Biotechnology and bioengineering, 103 (2009) 845-856.
[20] S. Piletsky, E. Piletska, A. Bossi, N. Turner, A. Turner, Surface functionalization of porous polypropylene membranes with polyaniline for protein immobilization, Biotechnology and bioengineering, 82 (2003) 86-92.
[21] D. Saeki, S. Nagao, I. Sawada, Y. Ohmukai, T. Maruyama, H. Matsuyama, Development of antibacterial polyamide reverse osmosis membrane modified with a covalently immobilized enzyme, Journal of membrane science, 428 (2013) 403-409.
[22] K. Hanušová, L. Vápenka, J. Dobiáš, L. Mišková, Development of antimicrobial packaging materials with immobilized glucose oxidase and lysozyme, Central European Journal of Chemistry, 11 (2013) 1066-1078.
[23] V. Muriel-Galet, J.N. Talbert, P. Hernandez-Munoz, R. Gavara, J. Goddard, Covalent immobilization of lysozyme on ethylene vinyl alcohol films for nonmigrating antimicrobial packaging applications, Journal of Agricultural and Food Chemistry, 61 (2013) 6720-6727.
[24] P. Goh, B. Ng, W. Lau, A. Ismail, Inorganic nanomaterials in polymeric ultrafiltration membranes for water treatment, Separation & Purification Reviews, 44 (2015) 216-249.
[25] S. Papageorgiou, F. Katsaros, E. Favvas, G.E. Romanos, C. Athanasekou, K. Beltsios, O. Tzialla, P. Falaras, Alginate fibers as photocatalyst immobilizing agents applied in hybrid photocatalytic/ultrafiltration water treatment processes, Water research, 46 (2012) 1858-1872.
[26] C. Xu, Y. Xu, J. Zhu, Photocatalytic antifouling graphene oxide-mediated hierarchical filtration membranes with potential applications on water purification, ACS applied materials & interfaces, 6 (2014) 16117-16123.
[27] B.S. Lalia, E. Guillen, H.A. Arafat, R. Hashaikeh, Nanocrystalline cellulose reinforced PVDF-HFP membranes for membrane distillation application, Desalination, 332 (2014) 134-141.
[28] M.A. Mohamed, W. Salleh, J. Jaafar, A. Ismail, M.A. Mutalib, S.M. Jamil, Incorporation of N-doped TiO 2 nanorods in regenerated cellulose thin films fabricated from recycled newspaper as a green portable photocatalyst, Carbohydrate polymers, 133 (2015) 429-437.
[29] M.A. Mohamed, W. Salleh, J. Jaafar, A. Ismail, M.A. Mutalib, N. Sani, S. Asri, C. Ong, Physicochemical characteristic of regenerated cellulose/N-doped TiO 2 nanocomposite membrane fabricated from recycled newspaper with photocatalytic activity under UV and visible light irradiation, Chemical Engineering Journal, 284 (2016) 202-215.
[30] T. Boccaccio, A. Bottino, G. Capannelli, P. Piaggio, Characterization of PVDF membranes by vibrational spectroscopy, Journal of membrane science, 210 (2002) 315-329.
[31] K. Khulbe, S. Gagne, A.T. Mohammadi, T. Matsuura, A.-M. Lamarche, Investigation of polymer morphology of integral-asymmetric membranes by ESR and Raman spectroscopy and its comparison with homogeneous films, Journal of membrane science, 98 (1995) 201-208.
[32] M. Mauricio-Iglesias, V. Guillard, N. Gontard, S. Peyron, Raman depth-profiling characterization of a migrant diffusion in a polymer, Journal of membrane science, 375 (2011) 165-171.
[33] K. Khulbe, T. Matsuura, S. Singh, G. Lamarche, S. Noh, Study on fouling of ultrafiltration membrane by electron spin resonance, Journal of membrane science, 167 (2000) 263-273.
[34] R.M. Stöckle, Y.D. Suh, V. Deckert, R. Zenobi, Nanoscale chemical analysis by tip-enhanced Raman spectroscopy, Chemical Physics Letters, 318 (2000) 131-136.
[35] B.-S. Yeo, J. Stadler, T. Schmid, R. Zenobi, W. Zhang, Tip-enhanced Raman Spectroscopy–Its status, challenges and future directions, Chemical Physics Letters, 472 (2009) 1-13.
[36] P.L. Stiles, J.A. Dieringer, N.C. Shah, R.P. Van Duyne, Surface-enhanced Raman spectroscopy, Annu. Rev. Anal. Chem., 1 (2008) 601-626.
[37] P.J. Pauzauskie, D. Talaga, K. Seo, P. Yang, F. Lagugné-Labarthet, Polarized Raman confocal microscopy of single gallium nitride nanowires, Journal of the American Chemical Society, 127 (2005) 17146-17147.

[38] U. Schmidt, S. Hild, W. Ibach, O. Hollricher, Characterization of thin polymer films on the nanometer scale with confocal Raman AFM, in: Macromolecular symposia, Wiley Online Library, 2005, pp. 133-143.
[39] E. Dufour, S. Gassara, E. Petit, C. Pochat-Bohatier, A. Deratani, Quantitative PVP mapping in PVDF hollow fiber membranes by using Raman spectroscopy coupled with spectral chemiometrics analysis, The European Physical Journal Special Topics, 224 (2015) 1911-1919.
[40] P. Menut, Y. Su, W. Chinpa, C. Pochat-Bohatier, A. Deratani, D. Wang, P. Huguet, C. Kuo, J. Lai, C. Dupuy, A top surface liquid layer during membrane formation using vapor-induced phase separation (VIPS)—Evidence and mechanism of formation, Journal of membrane science, 310 (2008) 278-288.
[41] X. Lu, P. Shah, S. Maruf, S. Ortiz, T. Hoffard, J. Pellegrino, Forensic analysis of degraded polypropylene hollow fibers utilized in microfiltration, Journal of Applied Polymer Science, 132 (2015).
[42] R. Lamsal, S.G. Harroun, C.L. Brosseau, G.A. Gagnon, Use of surface enhanced Raman spectroscopy for studying fouling on nanofiltration membrane, Separation and Purification Technology, 96 (2012) 7-11.
[43] P. Chen, L. Cui, K. Zhang, Surface-enhanced Raman spectroscopy monitoring the development of dual-species biofouling on membrane surfaces, Journal of membrane science, 473 (2015) 36-44.
[44] I. Patel, W. Premasiri, D. Moir, L. Ziegler, Barcoding bacterial cells: a SERS-based methodology for pathogen identification, Journal of Raman Spectroscopy, 39 (2008) 1660-1672.
[45] F. Bloch, W. Hansen, M. Packard, The Nuclear Induction Experiment, Physical Review, 70 (1946) 474.
[46] E.M. Purcell, H. Torrey, R.V. Pound, Resonance absorption by nuclear magnetic moments in a solid, Physical Review, 69 (1946) 37.
[47] K.K. Sadasivuni, J.-J. Cabibihan, M.A.S. Al-Maadeed, NMR spectroscopy of polymer nanocomposites, Spectroscopy of Polymer Nanocomposites, (2016) 181.
[48] J. Keeler, Understanding NMR Spectroscopy (2004), (2016).
[49] F. Heatley, Introduction to NMR and its use in the study of polymer stereochemistry, in: NMR spectroscopy of polymers, Springer, 1993, pp. 1-49.
[50] H.W. Spiess, Interplay of structure and dynamics in macromolecular and supramolecular systems, Macromolecules, 43 (2010) 5479-5491.
[51] D. Rana, T. Matsuura, K. Khulbe, C. Feng, Study on the spin probe added polymeric dense membranes by 13C solid-state nuclear magnetic resonance spectroscopy, Journal of Applied Polymer Science, 99 (2006) 3062-3069.
[52] A. Nechifor, V. Panait, L. Naftanaila, D. Batalu, S. Voicu, Symmetrically polysulfone membranes obtained by solvent evaporation using carbon nanotubes as additives. Synthesis, characterization and applications, Digest Journal of Nanomaterials and Biostructures, 8 (2013) 875-884.
[53] C.J. Rhodes, Electron Spin Resonance Spectroscopy: Principles and Instrumentation☆, in: Reference Module in Chemistry, Molecular Sciences and Chemical Engineering, Elsevier, 2016.
[54] K. Khulbe, G. Chowdhury, T. Matsuura, G. Lamarche, Characterization of PPO [poly (phenylene oxide)] powder and membranes from it by ESR technique, Journal of membrane science, 123 (1997) 9-15.
[55] K. Khulbe, G. Chowdhury, B. Kruczek, R. Vujosevic, T. Matsuura, G. Lamarche, Characterization of the PPO dense membrane prepared at different temperatures by ESR, atomic force microscope and gas permeation, Journal of membrane science, 126 (1997) 115-122.
[56] K. Khulbe, T. Matsuura, G. Lamarche, A.-M. Lamarche, C. Choi, S. Noh, Study of the structure of asymmetric cellulose acetate membranes for reverse osmosis using electron spin resonance (ESR) method, Polymer, 42 (2001) 6479-6484.
[57] K. Khulbe, T. Matsuura, C. Feng, Study on cellulose acetate membranes for reverse osmosis and polyethersulfone membranes for ultrafiltration by electron spin resonance technique, Desalination, 148 (2002) 329-332.

[58] K.C. Khulbea, C. Feng, T. Matsuura, G. Lamarche, A.M. Lamarche, Study of the structure and transport of asymmetric polyamide membranes for reverse osmosis using the electron spin resonance (ESR) method, Desalination, 154 (2003) 1-8.
[59] S.F. Oppenheim, G.R. Buettner, J.S. Dordick, V. Rodgers, Applying electron paramagnetic resonance spectroscopy to the study of fouling in protein ultrafiltration, Journal of membrane science, 96 (1994) 289-297.
[60] F.R. Oliveira, C.T. Matos, J.J. Moura, C.A. Portugal, J.G. Crespo, Study of membrane ageing and grafting mechanisms using electron paramagnetic resonance, Desalination and Water Treatment, 27 (2011) 150-158.
[61] Y.-N. Kwon, J.O. Leckie, Hypochlorite degradation of crosslinked polyamide membranes: I. Changes in chemical/morphological properties, Journal of membrane science, 283 (2006) 21-26.
[62] G.-D. Kang, C.-J. Gao, W.-D. Chen, X.-M. Jie, Y.-M. Cao, Q. Yuan, Study on hypochlorite degradation of aromatic polyamide reverse osmosis membrane, Journal of membrane science, 300 (2007) 165-171.
[63] A.F. Carley, D.J. Morgan, Surface Analysis: X-Ray Photoelectron Spectroscopy, in: Reference Module in Materials Science and Materials Engineering, Elsevier, 2016.
[64] M.C. Biesinger, B.P. Payne, A.P. Grosvenor, L.W. Lau, A.R. Gerson, R.S.C. Smart, Resolving surface chemical states in XPS analysis of first row transition metals, oxides and hydroxides: Cr, Mn, Fe, Co and Ni, Applied surface science, 257 (2011) 2717-2730.
[65] M. Ariza, J. Benavente, E. Rodriguez-Castellon, L. Palacio, Effect of hydration of polyamide membranes on the surface electrokinetic parameters: surface characterization by X-ray photoelectronic spectroscopy and atomic force microscopy, Journal of colloid and interface science, 247 (2002) 149-158.
[66] G.N.B. Baroña, M. Choi, B. Jung, High permeate flux of PVA/PSf thin film composite nanofiltration membrane with aluminosilicate single-walled nanotubes, Journal of colloid and interface science, 386 (2012) 189-197.
[67] X. Wei, B. Zhao, X.-M. Li, Z. Wang, B.-Q. He, T. He, B. Jiang, CF 4 plasma surface modification of asymmetric hydrophilic polyethersulfone membranes for direct contact membrane distillation, Journal of membrane science, 407 (2012) 164-175.
[68] P.S. Singh, V.K. Aswal, Compacted nanoscale blocks to build skin layers of reverse osmosis and nanofiltration membranes: A revelation from small-angle neutron scattering, The Journal of Physical Chemistry C, 111 (2007) 16219-16226.
[69] P. Fratzl, Small-angle scattering in materials science-a short review of applications in alloys, ceramics and composite materials, Journal of applied crystallography, 36 (2003) 397-404.
[70] P.S. Singh, G.L. Jadav, V.K. Aswal, A.K. Das, S. Kumar, A.M. Kansara, S.G. Chaudhri, H. Brahmbhatt, Comparison of the initial reactant structure and crosslinked network of poly (dimethyl siloxane) membranes from different macromonomers, Journal of Applied Polymer Science, 132 (2015).
[71] D. Johnson, S. Al Malek, B. Al-Rashdi, N. Hilal, Atomic force microscopy of nanofiltration membranes: effect of imaging mode and environment, Journal of membrane science, 389 (2012) 486-498.
[72] Y. Chang, T.-Y. Cheng, Y.-J. Shih, K.-R. Lee, J.-Y. Lai, Biofouling-resistance expanded poly (tetrafluoroethylene) membrane with a hydrogel-like layer of surface-immobilized poly (ethylene glycol) methacrylate for human plasma protein repulsions, Journal of membrane science, 323 (2008) 77-84.
[73] N. Park, B. Kwon, I.S. Kim, J. Cho, Biofouling potential of various NF membranes with respect to bacteria and their soluble microbial products (SMP): characterizations, flux decline, and transport parameters, Journal of membrane science, 258 (2005) 43-54.
[74] A.K. Singh, S. Prakash, V. Kulshrestha, V.K. Shahi, Cross-linked hybrid nanofiltration membrane with antibiofouling properties and self-assembled layered morphology, ACS applied materials & interfaces, 4 (2012) 1683-1692.

[75] A. Venault, Y. Chang, D.-M. Wang, D. Bouyer, A. Higuchi, J.-Y. Lai, PEGylation of anti-biofouling polysulfone membranes via liquid-and vapor-induced phase separation processing, Journal of membrane science, 403 (2012) 47-57.
[76] C.H. Worthley, K.T. Constantopoulos, M. Ginic-Markovic, R.J. Pillar, J.G. Matisons, S. Clarke, Surface modification of commercial cellulose acetate membranes using surface-initiated polymerization of 2-hydroxyethyl methacrylate to improve membrane surface biofouling resistance, Journal of membrane science, 385 (2011) 30-39.
[77] S. Al Malek, M.A. Seman, D. Johnson, N. Hilal, Formation and characterization of polyethersulfone membranes using different concentrations of polyvinylpyrrolidone, Desalination, 288 (2012) 31-39.
[78] B. Al-Rashdi, D. Johnson, N. Hilal, Removal of heavy metal ions by nanofiltration, Desalination, 315 (2013) 2-17.
[79] R.W. Carpick, D. Ogletree, M. Salmeron, Lateral stiffness: a new nanomechanical measurement for the determination of shear strengths with friction force microscopy, Applied Physics Letters, 70 (1997) 1548-1550.
[80] C.T. Gibson, G.S. Watson, S. Myhra, Lateral force microscopy—a quantitative approach, Wear, 213 (1997) 72-79.
[81] W.R. Bowen, N. Hilal, R.W. Lovitt, P.M. Williams, Atomic force microscope studies of membranes: surface pore structures of Diaflo ultrafiltration membranes, Journal of Colloid And Interface Science, 180 (1996) 350-359.
[82] P. Hansma, J. Cleveland, M. Radmacher, D. Walters, P. Hillner, M. Bezanilla, M. Fritz, D. Vie, H. Hansma, C. Prater, Tapping mode atomic force microscopy in liquids, Applied Physics Letters, 64 (1994) 1738-1740.
[83] H.G. Hansma, R.L. Sinsheimer, J. Groppe, T.C. Bruice, V. Elings, G. Gurley, M. Bezanilla, I.A. Mastrangelo, P.V. Hough, P.K. Hansma, Recent advances in atomic force microscopy of DNA, Scanning, 15 (1993) 296-299.
[84] Q. Zhong, D. Inniss, K. Kjoller, V. Elings, Fractured polymer/silica fiber surface studied by tapping mode atomic force microscopy, Surface Science Letters, 290 (1993) L688-L692.
[85] I. Schmitz, M. Schreiner, G. Friedbacher, M. Grasserbauer, Phase imaging as an extension to tapping mode AFM for the identification of material properties on humidity-sensitive surfaces, Applied surface science, 115 (1997) 190-198.
[86] R.S. McLean, B.B. Sauer, Tapping-mode AFM studies using phase detection for resolution of nanophases in segmented polyurethanes and other block copolymers, Macromolecules, 30 (1997) 8314-8317.
[87] M.E. Dokukin, I. Sokolov, Quantitative mapping of the elastic modulus of soft materials with HarmoniX and PeakForce QNM AFM modes, Langmuir, 28 (2012) 16060-16071.
[88] M. Shirazi, A. Kargari, S. Bazgir, M. Tabatabaei, M. Shirazi, M.S. Abdullah, T. Matsuura, A.F. Ismail, Characterization of electrospun polystyrene membrane for treatment of biodiesel's water-washing effluent using atomic force microscopy, Desalination, 329 (2013) 1-8.
[89] R. Garcıa, R. Perez, Dynamic atomic force microscopy methods, Surface Science Reports, 47 (2002) 197-301.
[90] F. Giessibl, Atomic resolution of the silicon (111)-(7× 7) surface by atomic force microscopy, Science, 267 (1995) 68-71.
[91] A. Weisenhorn, P. Maivald, H.-J. Butt, P. Hansma, Measuring adhesion, attraction, and repulsion between surfaces in liquids with an atomic-force microscope, Physical Review B, 45 (1992) 11226.
[92] W.R. Bowen, N. Hilal, R.W. Lovitt, C.J. Wright, An atomic force microscopy study of the adhesion of a silica sphere to a silica surface—effects of surface cleaning, Colloids and Surfaces A: Physicochemical and Engineering Aspects, 157 (1999) 117-125.
[93] M. Kappl, H.J. Butt, The colloidal probe technique and its application to adhesion force measurements, Particle & Particle Systems Characterization, 19 (2002) 129-143.

[94] C.J. Roberts, What can we learn from atomic force microscopy adhesion measurements with single drug particles?, European Journal of Pharmaceutical Sciences, 24 (2005) 153-157.
[95] J. Eve, N. Patel, S. Luk, S. Ebbens, C. Roberts, A study of single drug particle adhesion interactions using atomic force microscopy, International journal of pharmaceutics, 238 (2002) 17-27.
[96] X. Li, B.E. Logan, Analysis of bacterial adhesion using a gradient force analysis method and colloid probe atomic force microscopy, Langmuir, 20 (2004) 8817-8822.
[97] N.A. Burnham, D.D. Dominguez, R.L. Mowery, R.J. Colton, Probing the surface forces of monolayer films with an atomic-force microscope, Physical review letters, 64 (1990) 1931.
[98] M. Davies, A. Brindley, X. Chen, M. Marlow, S.W. Doughty, I. Shrubb, C.J. Roberts, Characterization of drug particle surface energetics and Young's modulus by atomic force microscopy and inverse gas chromatography, Pharmaceutical research, 22 (2005) 1158-1166.
[99] G. Gillies, M. Kappl, H.-J. Butt, Surface and capillary forces encountered by zinc sulfide microspheres in aqueous electrolyte, Langmuir, 21 (2005) 5882-5886.
[100] P.G. Hartley, F. Grieser, P. Mulvaney, G.W. Stevens, Surface forces and deformation at the oil-water interface probed using AFM force measurement, Langmuir, 15 (1999) 7282-7289.
[101] W.R. Bowen, N. Hilal, R.W. Lovitt, A.O. Sharif, P.M. Williams, Atomic force microscope studies of membranes: force measurement and imaging in electrolyte solutions, Journal of Membrane Science, 126 (1997) 77-89.
[102] S.K. Kaliappan, B. Cappella, Temperature dependent elastic–plastic behaviour of polystyrene studied using AFM force–distance curves, Polymer, 46 (2005) 11416-11423.
[103] J. Domke, M. Radmacher, Measuring the elastic properties of thin polymer films with the atomic force microscope, Langmuir, 14 (1998) 3320-3325.
[104] C. Plassard, E. Lesniewska, I. Pochard, A. Nonat, Investigation of the surface structure and elastic properties of calcium silicate hydrates at the nanoscale, Ultramicroscopy, 100 (2004) 331-338.
[105] A. Vinckier, I. Heyvaert, A. D'Hoore, T. McKittrick, C. Van Haesendonck, Y. Engelborghs, L. Hellemans, Immobilizing and imaging microtubules by atomic force microscopy, Ultramicroscopy, 57 (1995) 337-343.
[106] I. Dulińska, M. Targosz, W. Strojny, M. Lekka, P. Czuba, W. Balwierz, M. Szymoński, Stiffness of normal and pathological erythrocytes studied by means of atomic force microscopy, Journal of biochemical and biophysical methods, 66 (2006) 1-11.
[107] S. Allen, X. Chen, J. Davies, M.C. Davies, A.C. Dawkes, J.C. Edwards, C.J. Roberts, J. Sefton, S.J. Tendler, P.M. Williams, Detection of antigen-antibody binding events with the atomic force microscope, Biochemistry, 36 (1997) 7457-7463.
[108] R.B. Best, D.J. Brockwell, J.L. Toca-Herrera, A.W. Blake, D.A. Smith, S.E. Radford, J. Clarke, Force mode atomic force microscopy as a tool for protein folding studies, Analytica Chimica Acta, 479 (2003) 87-105.
[109] M. Rief, M. Gautel, F. Oesterhelt, J.M. Fernandez, H.E. Gaub, Reversible unfolding of individual titin immunoglobulin domains by AFM, Science, 276 (1997) 1109-1112.
[110] H.-J. Butt, B. Cappella, M. Kappl, Force measurements with the atomic force microscope: Technique, interpretation and applications, Surface Science Reports, 59 (2005) 1-152.
[111] D. Johnson, N. Hilal, Characterisation and quantification of membrane surface properties using atomic force microscopy: A comprehensive review, Desalination, 356 (2015) 149-164.
[112] D. Johnson, N. Hilal, W.R. Bowen, Basic principles of atomic force microscopy, Atomic force microscopy in process engineering: An introduction to AFM for improved processes and product, UK, IChemE, (2009).
[113] W.A. Ducker, T.J. Senden, R.M. Pashley, Direct measurement of colloidal forces using an atomic force microscope, Nature, 353 (1991) 239-241.
[114] N. Hilal, L. Al-Khatib, B.P. Atkin, V. Kochkodan, N. Potapchenko, Photochemical modification of membrane surfaces for (bio)fouling reduction: a nanoscale study using AFM, Desalination, 158 (2003) 65-72.

[115] K.H. Youm, W.S. Kim, Prediction of intrinsic pore properties of ultrafiltration membrane by solute rejection curves: effects of operating conditions on pore properties, Journal of chemical engineering of Japan, 24 (1991) 1-7.
[116] S. Singh, K. Khulbe, T. Matsuura, P. Ramamurthy, Membrane characterization by solute transport and atomic force microscopy, Journal of membrane science, 142 (1998) 111-127.
[117] M. Khayet, C. Feng, K. Khulbe, T. Matsuura, Preparation and characterization of polyvinylidene fluoride hollow fiber membranes for ultrafiltration, Polymer, 43 (2002) 3879-3890.
[118] K. Kaneko, Determination of pore size and pore size distribution: 1. Adsorbents and catalysts, Journal of membrane science, 96 (1994) 59-89.
[119] J. Stawikowska, A.G. Livingston, Assessment of atomic force microscopy for characterisation of nanofiltration membranes, Journal of membrane science, 425 (2013) 58-70.
[120] A. Matin, H. Shafi, Z. Khan, M. Khaled, R. Yang, K. Gleason, F. Rehman, Surface modification of seawater desalination reverse osmosis membranes: characterization studies & performance evaluation, Desalination, 343 (2014) 128-139.
[121] B.M. Borkent, S. de Beer, F. Mugele, D. Lohse, On the shape of surface nanobubbles, Langmuir, 26 (2009) 260-268.
[122] N. Ishida, T. Inoue, M. Miyahara, K. Higashitani, Nano bubbles on a hydrophobic surface in water observed by tapping-mode atomic force microscopy, Langmuir, 16 (2000) 6377-6380.
[123] P. Attard, Nanobubbles and the hydrophobic attraction, Advances in Colloid and Interface Science, 104 (2003) 75-91.
[124] H.K. Christenson, P.M. Claesson, Direct measurements of the force between hydrophobic surfaces in water, Advances in Colloid and Interface Science, 91 (2001) 391-436.
[125] V. Kochkodan, Y. Manawi, D.J. Johnson, A.K. Fard, M. Atieh, Surface modification of polyamide membranes using the layer-by-layer technique: Characterization and antifouling potential, Desalination and Water Treatment, In Press (2017).
[126] P. Kaner, D.J. Johnson, E. Seker, N. Hilal, S.A. Altinkaya, Layer-by-layer surface modification of polyethersulfone membranes using polyelectrolytes and AgCl/TiO 2 xerogels, Journal of membrane science, 493 (2015) 807-819.
[127] B. Mi, M. Elimelech, Silica scaling and scaling reversibility in forward osmosis, Desalination, 312 (2013) 75-81.
[128] E. Guillen-Burrieza, R. Thomas, B. Mansoor, D. Johnson, N. Hilal, H. Arafat, Effect of dry-out on the fouling of PVDF and PTFE membranes under conditions simulating intermittent seawater membrane distillation (SWMD), Journal of membrane science, 438 (2013) 126-139.
[129] H.H. Rijnaarts, W. Norde, E.J. Bouwer, J. Lyklema, A.J. Zehnder, Bacterial adhesion under static and dynamic conditions, Applied and Environmental Microbiology, 59 (1993) 3255-3265.
[130] D. Johnson, F. Galiano, S.A. Deowan, J. Hoinkis, A. Figoli, N. Hilal, Adhesion forces between humic acid functionalized colloidal probes and polymer membranes to assess fouling potential, Journal of membrane science, 484 (2015) 35-46.
[131] F. Galiano, A. Figoli, S.A. Deowan, D. Johnson, S.A. Altinkaya, L. Veltri, G. De Luca, R. Mancuso, N. Hilal, B. Gabriele, A step forward to a more efficient wastewater treatment by membrane surface modification via polymerizable bicontinuous microemulsion, Journal of membrane science, 482 (2015) 103-114.
[132] S. Deowan, B. Wagner, C. Aresipathi, J. Hoinkis, A. Figoli, E. Drioli, Treatment of Model Textile Dye Wastewater (MTDW) Towards Developing Novel Submerged Membrane Bioreactor Process, Procedia Engineering, 44 (2012) 1768-1771.
[133] B. Tansel, J. Sager, J. Garland, S. Xu, L. Levine, P. Bisbee, Deposition of extracellular polymeric substances (EPS) and microtopographical changes on membrane surfaces during intermittent filtration conditions, Journal of membrane science, 285 (2006) 225-231.
[134] X. Su, Y. Tian, W. Zuo, J. Zhang, H. Li, X. Pan, Static adsorptive fouling of extracellular polymeric substances with different membrane materials, Water research, 50 (2014) 267-277.

[135] W.R. Bowen, N. Hilal, R.W. Lovitt, C.J. Wright, Direct measurement of interactions between adsorbed protein layers using an atomic force microscope, Journal of colloid and interface science, 197 (1998) 348-352.
[136] W.R. Bowen, N. Hilal, R.W. Lovitt, C.J. Wright, Characterisation of membrane surfaces: direct measurement of biological adhesion using an atomic force microscope, Journal of membrane science, 154 (1999) 205-212.
[137] M. Herzberg, S. Kang, M. Elimelech, Role of extracellular polymeric substances in biofouling of reverse osmosis membranes, Environmental Science & Technology, 43 (2009) 4393-4398.
[138] R. Bernstein, S. Belfer, V. Freger, Bacterial attachment to RO membranes surface-modified by concentration-polarization-enhanced graft polymerization, Environmental Science & Technology, 45 (2011) 5973-5980.
[139] A. Zaky, I. Escobar, A.M. Motlagh, C. Gruden, Determining the influence of active cells and conditioning layer on early stage biofilm formation using cellulose acetate ultrafiltration membranes, Desalination, 286 (2012) 296-303.
[140] L. Chen, Y. Tian, C.-q. Cao, J. Zhang, Z.-n. Li, Interaction energy evaluation of soluble microbial products (SMP) on different membrane surfaces: role of the reconstructed membrane topology, Water research, 46 (2012) 2693-2704.
[141] W. Zhou, R. Apkarian, Z.L. Wang, D. Joy, Fundamentals of Scanning Electron Microscopy (SEM), in: Scanning Microscopy for Nanotechnology, Springer, 2006, pp. 1-40.
[142] J. Goldstein, D. Newbury, P. Echlin, D. Joy, C. Fiori, E. Lifshin, Scanning electron microscopy and X-ray microanalysis. A text for biologists, materials scientists, and geologists, Scanning electron microscopy and X-ray microanalysis. A text for biologists, materials scientists, and geologists., (1981).
[143] J. Jerosch, R. Reichelt, Scanning electron microscopy studies of morphologic changes in chemically stabilized ultrahigh molecular weight polyethylene, Biomedizinische Technik. Biomedical engineering, 42 (1997) 358-362.
[144] A.J. Bromley, R.G. Holdich, I.W. Cumming, Particulate fouling of surface microfilters with slotted and circular pore geometry, Journal of membrane science, 196 (2002) 27-37.
[145] Y. Wang, J. Zhu, H. Huang, H.-H. Cho, Carbon nanotube composite membranes for microfiltration of pharmaceuticals and personal care products: Capabilities and potential mechanisms, Journal of membrane science, 479 (2015) 165-174.
[146] M.G. Buonomenna, E. Drioli, R. Bertoncello, L. Milanese, L.J. Prins, P. Scrimin, G. Licini, Ti (IV)/trialkanolamine catalytic polymeric membranes: Preparation, characterization, and use in oxygen transfer reactions, Journal of Catalysis, 238 (2006) 221-231.
[147] J.G. Wen, Transmission Electron Microscopy, in: M. Sardela (Ed.) Practical Materials Characterization, Springer New York, New York, NY, 2014, pp. 189-229.
[148] C.Y. Tang, Z. Yang, Transmission Electron Microscope, in: N. Hilal, A. Ismail, T. Matsuura, D. Oatkey-Radcliffe (Eds.) Membrane Characterization, Elsevier, 2017.
[149] V. Freger, J. Gilron, S. Belfer, TFC polyamide membranes modified by grafting of hydrophilic polymers: an FT-IR/AFM/TEM study, Journal of membrane science, 209 (2002) 283-292.
[150] B.-H. Jeong, E.M. Hoek, Y. Yan, A. Subramani, X. Huang, G. Hurwitz, A.K. Ghosh, A. Jawor, Interfacial polymerization of thin film nanocomposites: a new concept for reverse osmosis membranes, Journal of membrane science, 294 (2007) 1-7.
[151] F.A. Pacheco, I. Pinnau, M. Reinhard, J.O. Leckie, Characterization of isolated polyamide thin films of RO and NF membranes using novel TEM techniques, Journal of membrane science, 358 (2010) 51-59.
[152] F. Pacheco, R. Sougrat, M. Reinhard, J.O. Leckie, I. Pinnau, 3D visualization of the internal nanostructure of polyamide thin films in RO membranes, Journal of membrane science, 501 (2016) 33-44.
[153] V. Gekas, K.M. Persson, M. Wahlgren, B. Sivik, Contact angles of ultrafiltration membranes and their possible correlation to membrane performance, Journal of membrane science, 72 (1992) 293-302.

[154] M. Rosa, M. De Pinho, Membrane surface characterisation by contact angle measurements using the immersed method, Journal of membrane science, 131 (1997) 167-180.
[155] T. Young, An essay on the cohesion of fluids, Philosophical Transactions of the Royal Society of London, 95 (1805) 65-87.
[156] G. Whyman, E. Bormashenko, T. Stein, The rigorous derivation of Young, Cassie–Baxter and Wenzel equations and the analysis of the contact angle hysteresis phenomenon, Chemical Physics Letters, 450 (2008) 355-359.
[157] D.J. Johnson, N.J. Miles, N. Hilal, Quantification of particle–bubble interactions using atomic force microscopy: A review, Advances in Colloid and Interface Science, 127 (2006) 67-81.
[158] D. Kwok, C. Lam, A. Li, A. Leung, R. Wu, E. Mok, A. Neumann, Measuring and interpreting contact angles: a complex issue, Colloids and Surfaces A: Physicochemical and Engineering Aspects, 142 (1998) 219-235.
[159] H. Tavana, C. Lam, K. Grundke, P. Friedel, D. Kwok, M. Hair, A. Neumann, Contact angle measurements with liquids consisting of bulky molecules, Journal of colloid and interface science, 279 (2004) 493-502.
[160] H. Eral, J. Oh, Contact angle hysteresis: a review of fundamentals and applications, Colloid and polymer science, 291 (2013) 247-260.
[161] E. De Souza, L. Gao, T. McCarthy, E. Arzt, A. Crosby, Effect of contact angle hysteresis on the measurement of capillary forces, Langmuir, 24 (2008) 1391-1396.
[162] L. Gao, T.J. McCarthy, Contact angle hysteresis explained, Langmuir, 22 (2006) 6234-6237.
[163] B. He, J. Lee, N.A. Patankar, Contact angle hysteresis on rough hydrophobic surfaces, Colloids and Surfaces A: Physicochemical and Engineering Aspects, 248 (2004) 101-104.
[164] R.N. Wenzel, Surface Roughness and Contact Angle, The Journal of Physical Chemistry, 53 (1949) 1466-1467.
[165] A. Milne, A. Amirfazli, The Cassie equation: How it is meant to be used, Advances in Colloid and Interface Science, 170 (2012) 48-55.
[166] A. Cassie, S. Baxter, Wettability of porous surfaces, Transactions of the Faraday Society, 40 (1944) 546-551.
[167] E. Bormashenko, Why does the Cassie–Baxter equation apply?, Colloids and Surfaces A: Physicochemical and Engineering Aspects, 324 (2008) 47-50.
[168] J. Drelich, J.D. Miller, R.J. Good, The effect of drop (bubble) size on advancing and receding contact angles for heterogeneous and rough solid surfaces as observed with sessile-drop and captive-bubble techniques, Journal of colloid and interface science, 179 (1996) 37-50.
[169] W. Zhang, M. Wahlgren, B. Sivik, Membrane characterization by the contact angle technique: II. Characterization of UF-membranes and comparison between the captive bubble and sessile drop as methods to obtain water contact angles, Desalination, 72 (1989) 263-273.
[170] L. Románszki, M. Mohos, J. Telegdi, Z. Keresztes, L. Nyikos, A comparison of contact angle measurement results obtained on bare, treated, and coated alloy samples by both dynamic sessile drop and Wilhelmy method, Periodica Polytechnica. Chemical Engineering, 58 (2014) 53.
[171] J.W. Bullard, E.J. Garboczi, Capillary rise between planar surfaces, Physical Review E, 79 (2009) 011604.
[172] M. Ulbricht, Advanced functional polymer membranes, Polymer, 47 (2006) 2217-2262.
[173] V. Kochkodan, N. Hilal, A comprehensive review on surface modified polymer membranes for biofouling mitigation, Desalination, 356 (2015) 187-207.
[174] R.S. Hebbar, A.M. Isloor, A.F. Ismail, Contact Angle Measurements, in: N. Hilal, A. Ismail, T. Matsuura, D. Oatkey-Radcliffe (Eds.) Membrane Characterization, Elsevier, 2007.
[175] M.d.C. García-Payo, M.A. Izquierdo-Gil, C. Fernández-Pineda, Wetting study of hydrophobic membranes via liquid entry pressure measurements with aqueous alcohol solutions, Journal of colloid and interface science, 230 (2000) 420-431.

[176] L. Li, Z. Yin, F. Li, T. Xiang, Y. Chen, C. Zhao, Preparation and characterization of poly (acrylonitrile-acrylic acid-N-vinyl pyrrolidinone) terpolymer blended polyethersulfone membranes, Journal of membrane science, 349 (2010) 56-64.
[177] X. Chen, J. Luo, B. Qi, W. Cao, Y. Wan, NOM fouling behavior during ultrafiltration: Effect of membrane hydrophilicity, Journal of Water Process Engineering, 7 (2015) 1-10.
[178] R. Kumar, A.M. Isloor, A.F. Ismail, S.A. Rashid, A. Al Ahmed, Permeation, antifouling and desalination performance of TiO 2 nanotube incorporated PSf/CS blend membranes, Desalination, 316 (2013) 76-84.
[179] R. Kumar, A.M. Isloor, A.F. Ismail, T. Matsuura, Performance improvement of polysulfone ultrafiltration membrane using N-succinyl chitosan as additive, Desalination, 318 (2013) 1-8.
[180] M. Khayet, T. Matsuura, Application of surface modifying macromolecules for the preparation of membranes for membrane distillation, Desalination, 158 (2003) 51-56.
[181] A. Al-Amoudi, P. Williams, A. Al-Hobaib, R.W. Lovitt, Cleaning results of new and fouled nanofiltration membrane characterized by contact angle, updated DSPM, flux and salts rejection, Applied surface science, 254 (2008) 3983-3992.
[182] R. Hunter, Zeta Potential in Colloid Science Academic, New York, (1981) 69.
[183] D. Möckel, E. Staude, M. Dal-Cin, K. Darcovich, M. Guiver, Tangential flow streaming potential measurements: hydrodynamic cell characterization and zeta potentials of carboxylated polysulfone membranes, Journal of membrane science, 145 (1998) 211-222.
[184] D. Oatley-Radcliffe, N. Aljohani, P.M. Williams, N. Hilal, Electrokinetic Phenomena for Membrane Charge, in: N. Hilal, A. Ismail, T. Matsuura, D. Oatley-Radcliffe (Eds.), Elsevier, 2017.
[185] Á.V. Delgado, F. González-Caballero, R. Hunter, L. Koopal, J. Lyklema, Measurement and interpretation of electrokinetic phenomena, Journal of colloid and interface science, 309 (2007) 194-224.
[186] M. Elimelech, W.H. Chen, J.J. Waypa, Measuring the zeta (electrokinetic) potential of reverse osmosis membranes by a streaming potential analyzer, Desalination, 95 (1994) 269-286.
[187] J. Lyklema, Fundamentals of Interface and Colloid Science: Part II Solid-Fluid Interfaces, Academic Press, London, 1996.
[188] J. Peeters, M. Mulder, H. Strathmann, Streaming potential measurements as a characterization method for nanofiltration membranes, Colloids and Surfaces A: Physicochemical and Engineering Aspects, 150 (1999) 247-259.
[189] N. Ding, X.-L. Wang, J. Wang, Electrokinetic phenomena of a polyethylene microfiltration membrane in single salt solutions of NaCl, KCl, MgCl 2, Na 2 SO 4, and MgSO 4, Desalination, 192 (2006) 18-24.
[190] L. Ricq, A. Pierre, S. Bayle, J.-C. Reggiani, Electrokinetic characterization of polyethersulfone UF membranes, Desalination, 109 (1997) 253-261.
[191] M. Ariza, J. Benavente, Streaming potential along the surface of polysulfone membranes: a comparative study between two different experimental systems and determination of electrokinetic and adsorption parameters, Journal of membrane science, 190 (2001) 119-132.
[192] M.W. Verbrugge, P.N. Pintauro, Transport models for ion-exchange membranes, in: B.E. Conway, J.O.M. Bockris, R.E. White (Eds.) Modern Aspects of Electrochemistry, Plenum Press, New York and London, 1989, pp. 1-64.
[193] M. Kukizaki, Relation between salt rejection and electrokinetic properties on Shirasu porous glass (SPG) membranes with nano-order uniform pores, Separation and Purification Technology, 69 (2009) 87-96.
[194] H. Bukšek, T. Luxbacher, I. Petrinić, Zeta potential determination of polymeric materials using two differently designed measuring cells of an electrokinetic analyzer, Acta Chim. Slov, 57 (2010) 700-706.
[195] W.R. Bowen, R.A. Clark, Electro-osmosis at microporous membranes and the determination of zeta-potential, Journal of colloid and interface science, 97 (1984) 401-409.

[196] A. Szymczyk, P. Fievet, M. Mullet, J. Reggiani, J. Pagetti, Comparison of two electrokinetic methods–electroosmosis and streaming potential–to determine the zeta-potential of plane ceramic membranes, Journal of membrane science, 143 (1998) 189-195.
[197] A. Szymczyk, P. Fievet, M. Mullet, J.C. Reggiani, J. Pagetti, Study of electrokinetic properties of plate ceramic membranes by electroosmosis and streaming potential, Desalination, 119 (1998) 309-313.
[198] K.J. Kim, A.G. Fane, M. Nystrom, A. Pihlajamaki, W.R. Bowen, H. Mukhtar, Evaluation of electroosmosis and streaming potential for measurement of electric charges of polymeric membranes, Journal of membrane science, 116 (1996) 149-159.
[199] P. Narong, A. James, Sodium chloride rejection by a UF ceramic membrane in relation to its surface electrical properties, Separation and Purification Technology, 49 (2006) 122-129.
[200] L. Ricq, A. Pierre, J.-C. Reggiani, J. Pagetti, A. Foissy, Use of electrophoretic mobility and streaming potential measurements to characterize electrokinetic properties of ultrafiltration and microfiltration membranes, Colloids and Surfaces A: Physicochemical and Engineering Aspects, 138 (1998) 301-308.
[201] C. Bellona, J.E. Drewes, The role of membrane surface charge and solute physico-chemical properties in the rejection of organic acids by NF membranes, Journal of membrane science, 249 (2005) 227-234.
[202] W.Y. Wang, Y. Ku, Effects of solution pH and UV irradiation on the streaming potential of the titanium dioxide membranes, Journal of membrane science, 282 (2006) 342-350.
[203] T.E. Thomas, S.A. Aani, D.L. Oatley-Radcliffe, P.M. Williams, N. Hilal, Laser Doppler Electrophoresis and electro-osmotic flow mapping: A novel methodology for the determination of membrane surface zeta potential, Journal of membrane science, 523 (2017) 524-532.

Figure Captions

Figure 1: Basic operation of ATR-FTIR system.

Figure 2: Spectra of polysulfone / poly ether sulfone blended membranes. Reproduced from [3] with permission. Copyright 2015, John Wily and Sons.

Figure 3 ATR-FTIR spectra of polypropylene membranes treated with Freon-116 plasma. Reproduced from [12] with permission. Copyright 2001, Elsevier.

Figure 4: Transmission FTIR spectra of PES membranes treated with polyacrylic acid in Argon plasms: a) unmodified membrane; b) grafting yield (GY) = 85 μg/cm^2; c) GY = 155 μg/cm^2; d) GY = 162 μg/cm^2; e) GY = 210 μg/cm^2. Reproduced from [13] with permission. Copyright 2002 Elsevier.

Figure 5: ATR-FTIR spectra of pristine and modified membranes. M5, M10 and M12 membranes modified with grafting densities of 1.17. 0.60 and 0.43 mg/cm2 respectively. Reproduced with permission from [17]. Copyright 2015, Elsevier.

Figure 6: SERS spectra of virgin, fouled and cleaned membrane samples. Reproduced with permission from [42]. Copyright 2015, Elsevier

Figure 7: NMR spectrum of PSF membranes containing CNTS functionalised with amino-benzo crown ether. Reproduced with permission from [52]. Copyright 2013 Virtual Company of Physics S.R.L

Figure 8: XPS spectra for NF45 and B0 membranes. Reproduced with permission from [65]. Copyright 2000, Elsevier.

Figure 9: Example AFM force-distance curve showing approach (red trace) and retract (blue trace).

Figure 10: Globular features only seen with tapping mode in water on hydrophobic surface (a) – not with contact mode in water (b). Images reproduced from Johnson *et al* [71] with permission. Copyright Elsevier 2012.

Figure 11: AFM scans of NF90 membrane: virgin membrane a); and layer-by-layer modified samples with a different number of PSScoMA/ PEI layers: b) - 4 layers; c) – 8 layers; d) – 12 layers.

Figure 12: SEM surface image (a) and cross-section (b–d) of PBM membrane with magnification from ×10,000 to ×40,000. Reproduced from Galiano *et al* [131] with permission. Copyright Elsevier 2015.

Figures

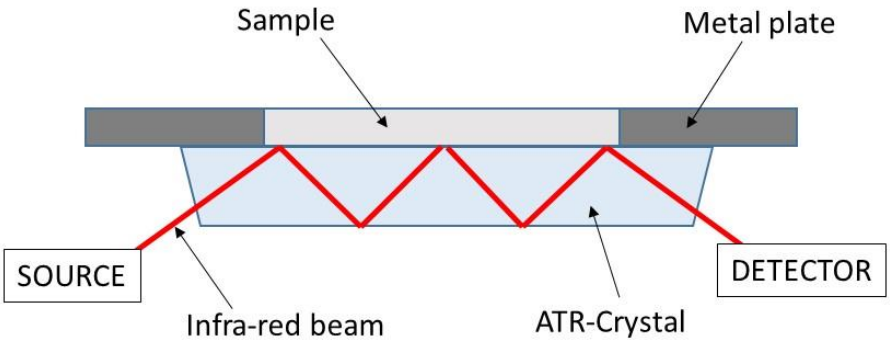

Figure 1

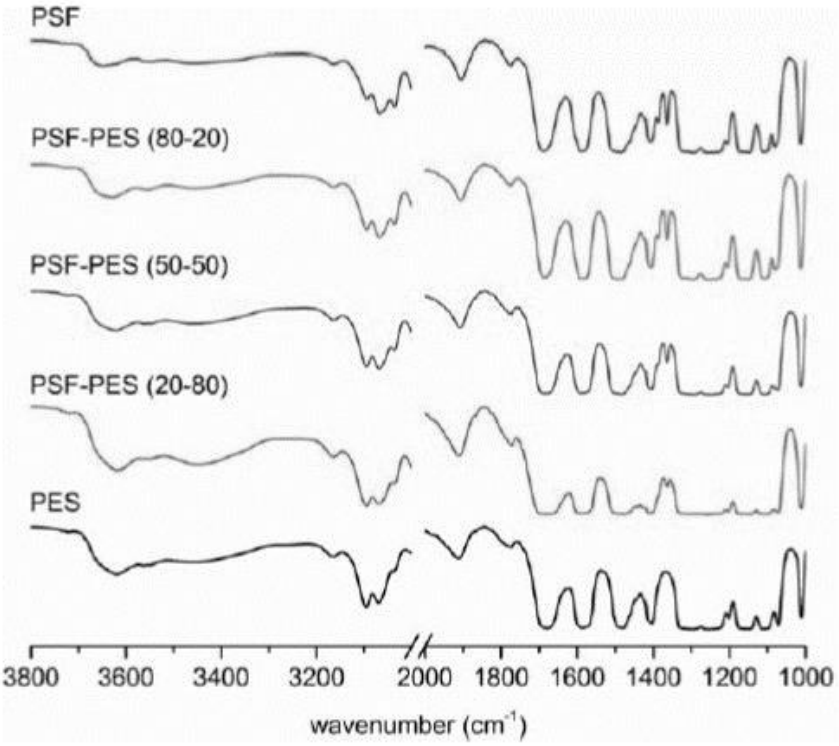
PSF
PSF-PES (80-20)
PSF-PES (50-50)
PSF-PES (20-80)
PES
3800
3600
3400
3200
2000
1800
1600
1400
1200
1000
wavenumber (cm-1)

Figure 2

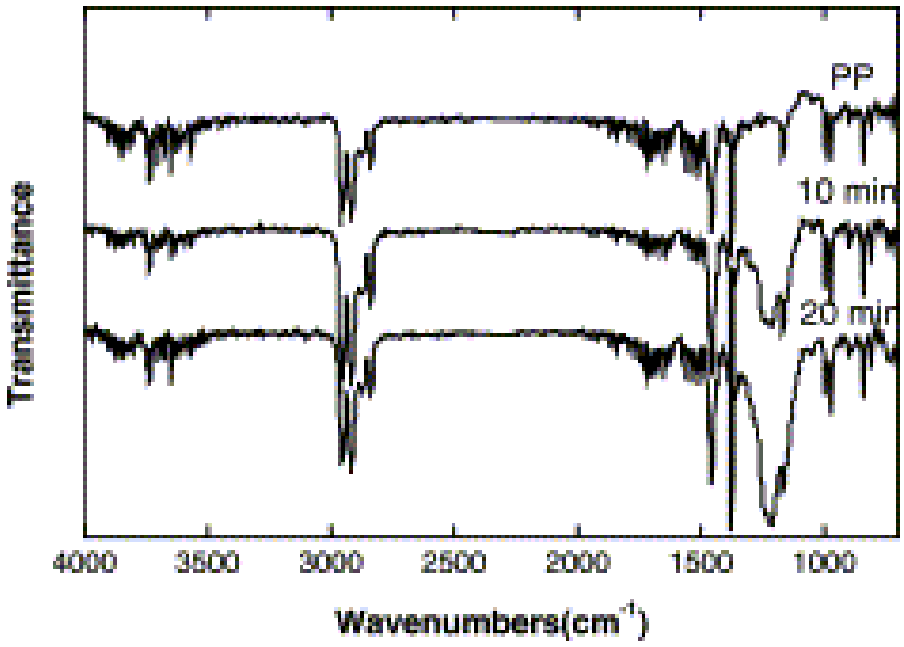
PP
10 min
20 min
Transmittance
4000
3500
3000
2500
2000
1500
1000
Wavenumbers(cm-1)

Figure 3

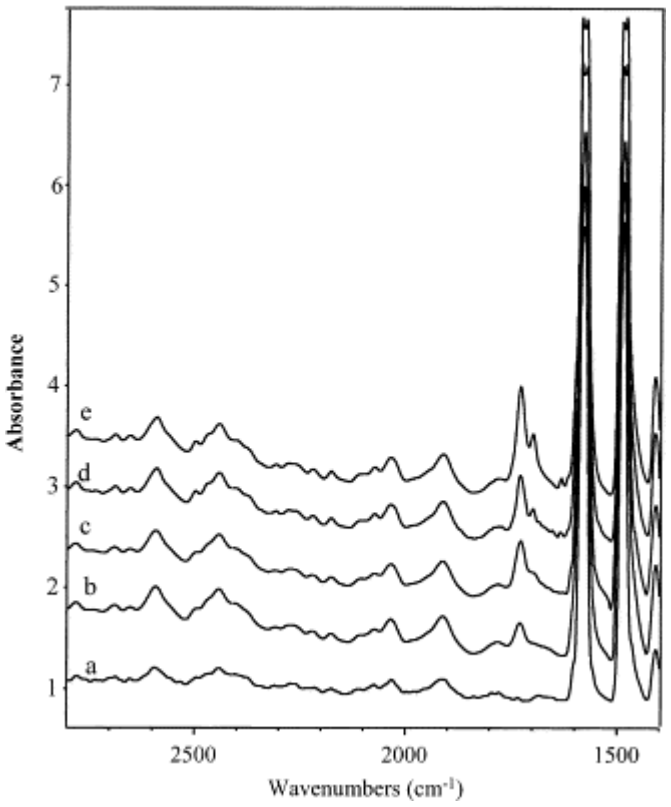

Figure 4

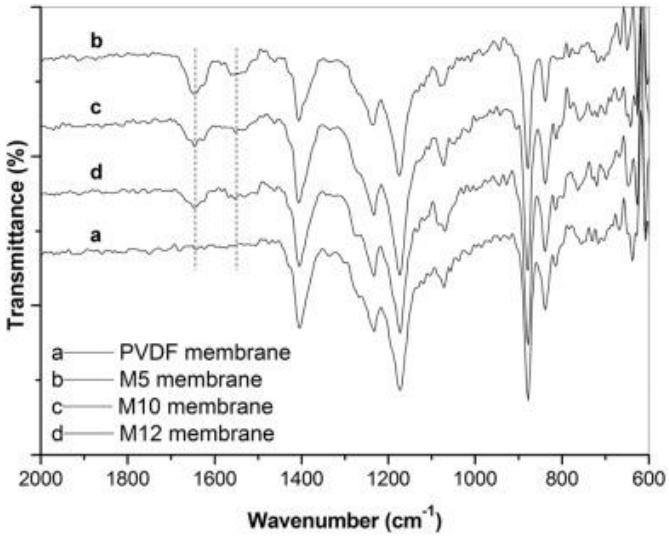
b
c
d
a
Transmittance (%)
a PVDF membrane
b M5 membrane
c M10 membrane
d M12 membrane
2000
1800
1600
1400
1200
1000
800
600
Wavenumber (cm-1)

Figure 5

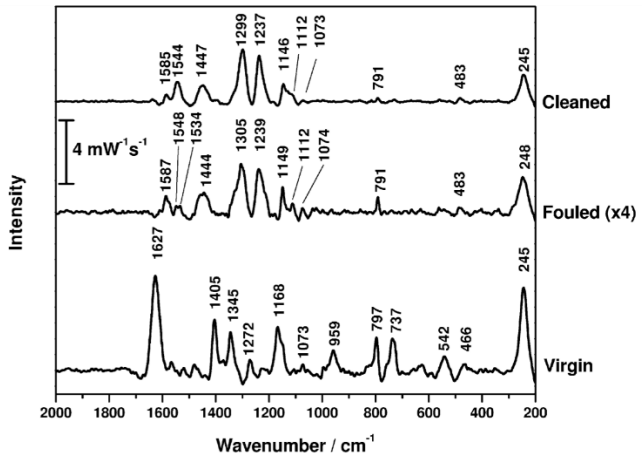
Intensity
4 mW^{-1}s^{-1}
1585
1544
1447
1299
1237
1146
1112
1073
791
483
245
Cleaned
1587
1548
1534
1444
1305
1239
1149
1112
1074
791
483
248
Fouled (x4)
1627
1405
1345
1272
1168
1073
959
797
737
542
466
245
Virgin
2000
1800
1600
1400
1200
1000
800
600
400
200
Wavenumber / cm^{-1}

Figure 6

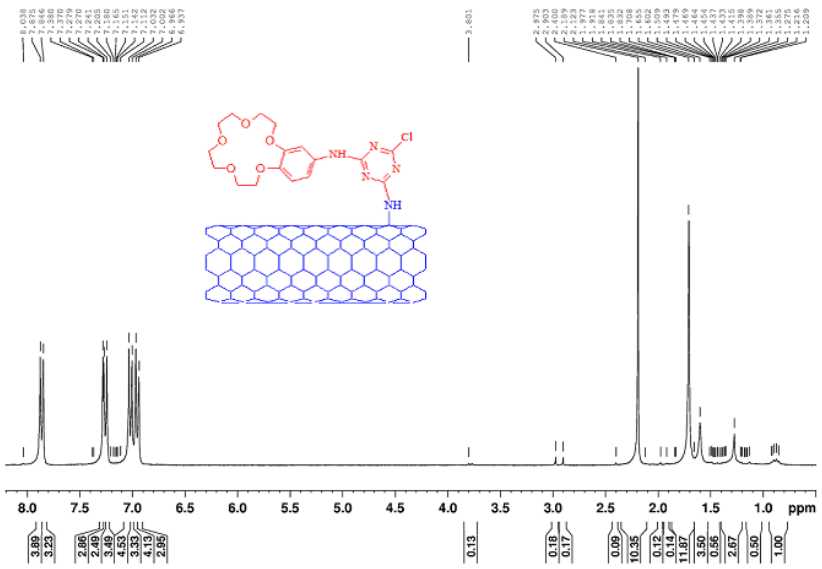

Figure 7

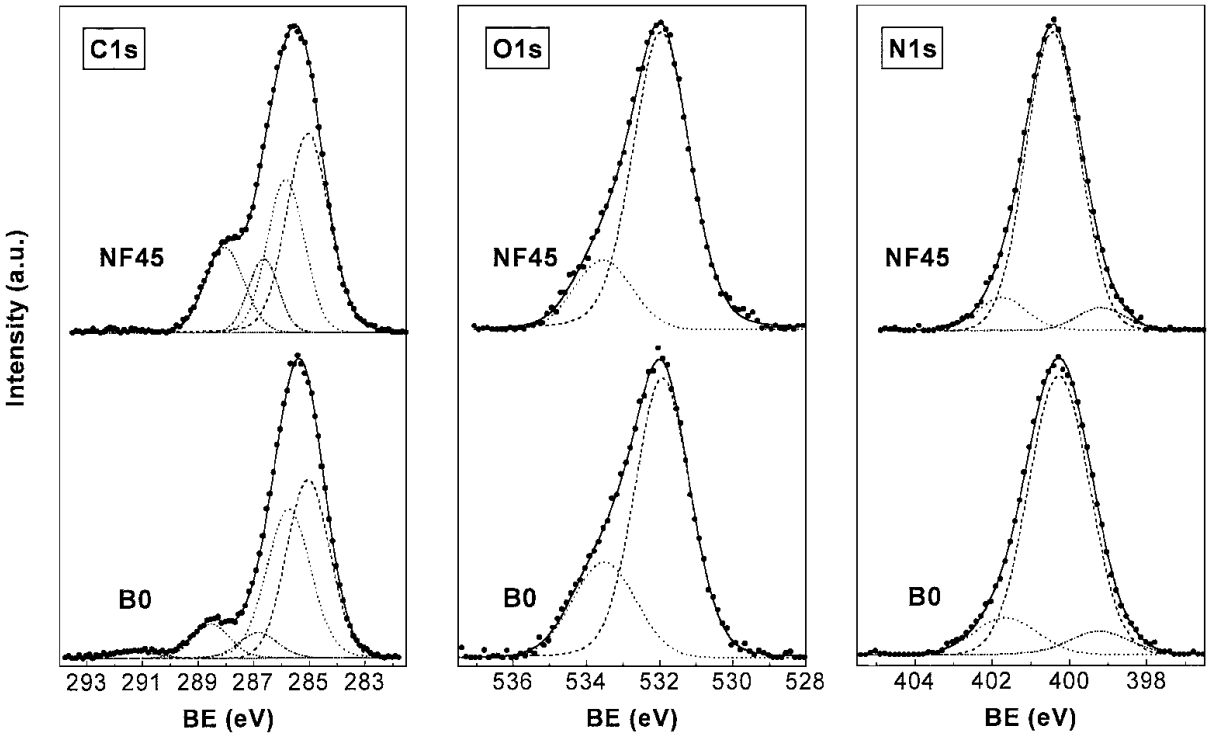
C1s
O1s
N1s
NF45
B0
Intensity (a.u.)
293 291 289 287 285 283
536 534 532 530 528
404 402 400 398
BE (eV)

Figure 8

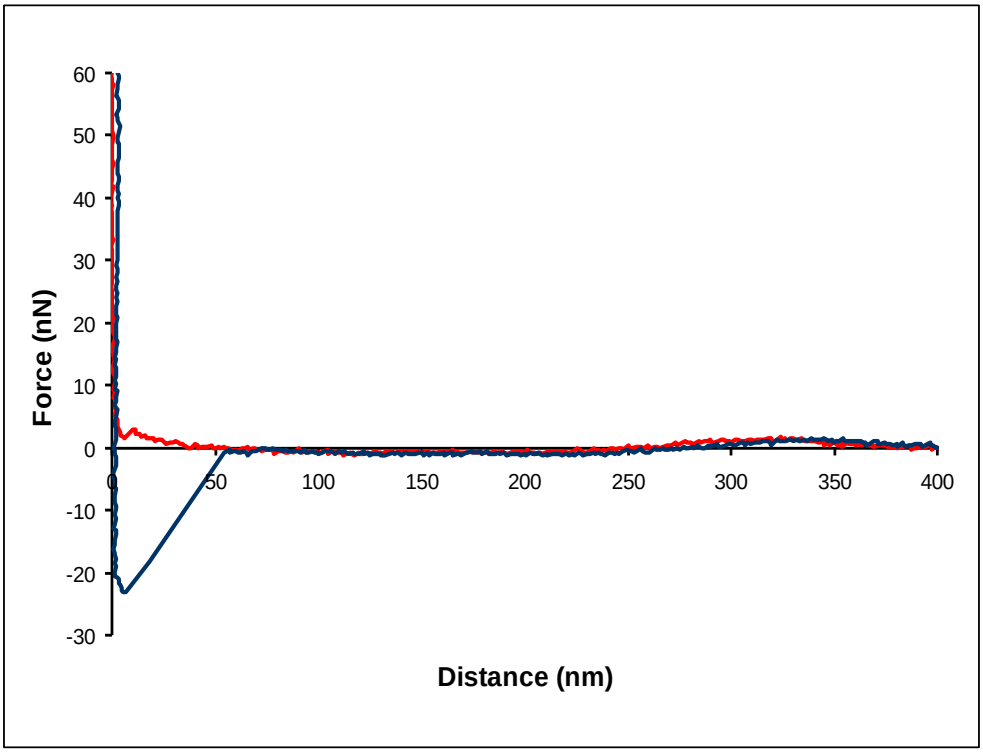
60
50
40
30
20
10
0
-10
-20
-30
Force (nN)
0
50
100
150
200
250
300
350
400
Distance (nm)

Figure 9

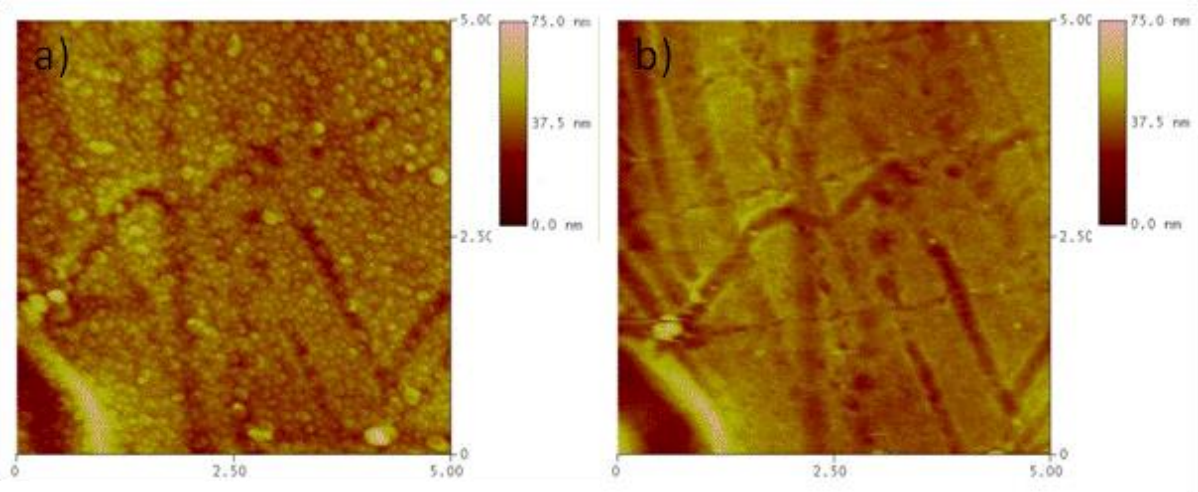

Figure 10

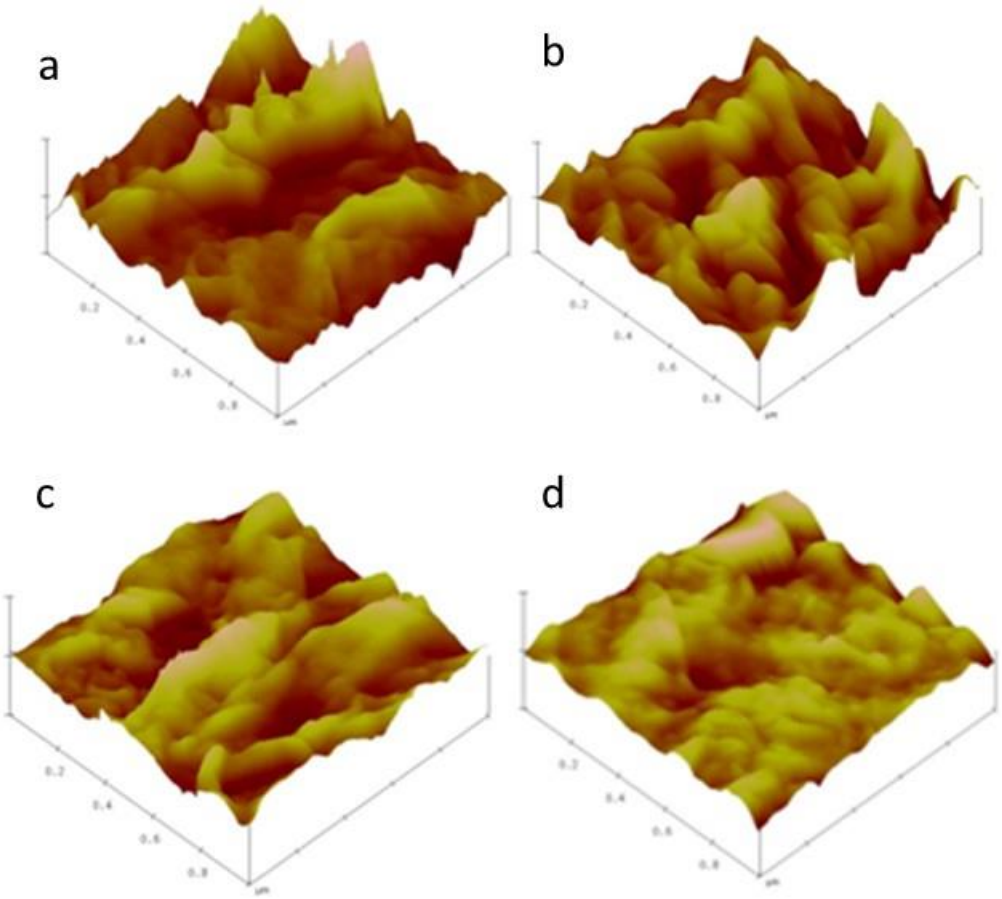

Figure 11

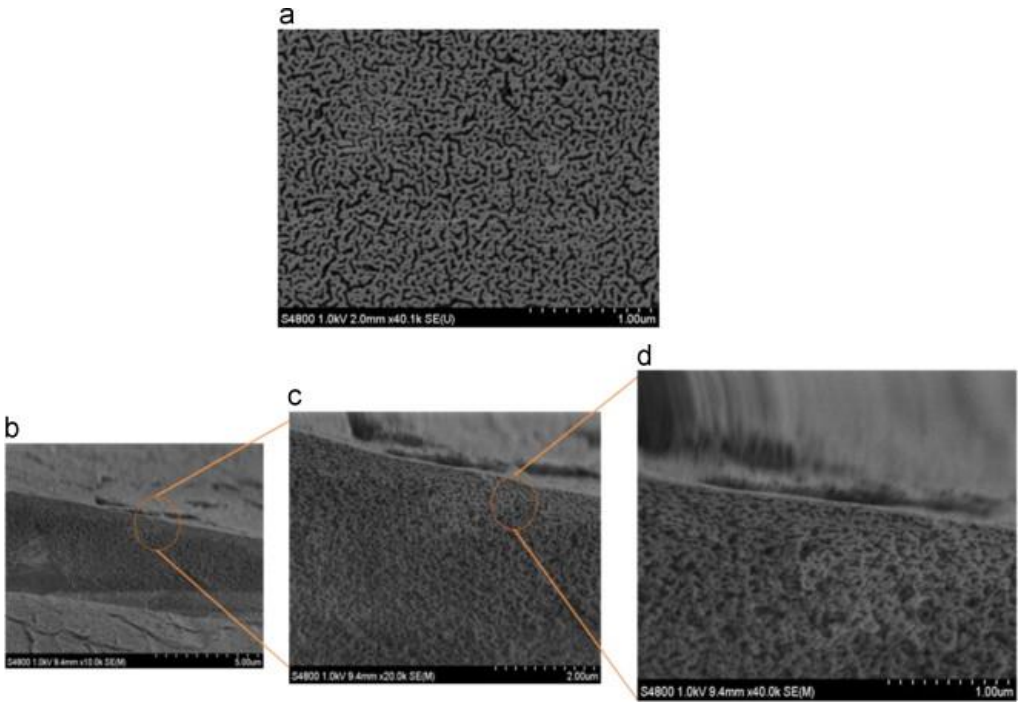
a
S4800 1.0kV 2.0mm x40.1k SE(U)
1.00um
b
c
d
S4800 1.0kV 9.4mm x20.0k SE(M)
2.00um
S4800 1.0kV 9.4mm x40.0k SE(M)
1.00um

Figure 12

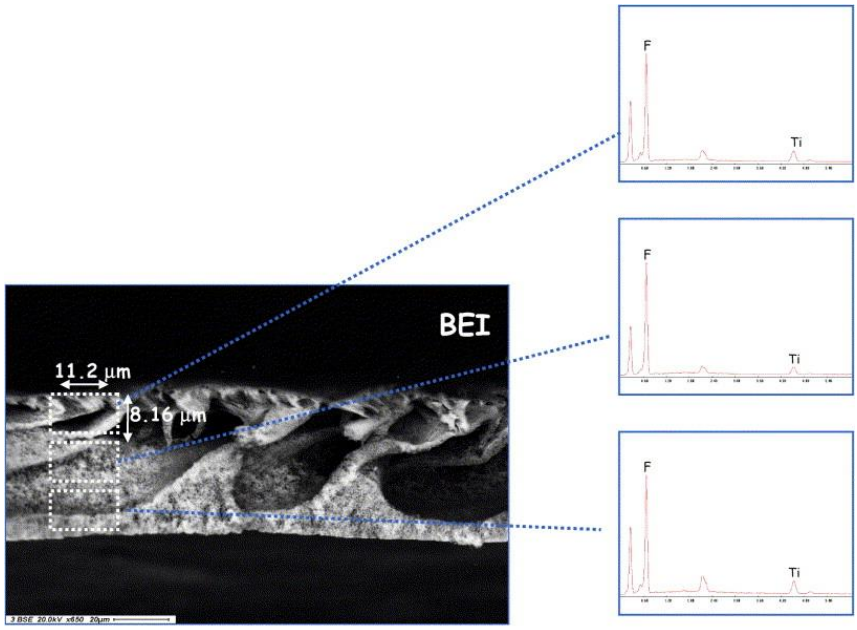

a) b)

Figure 13

a)

b)

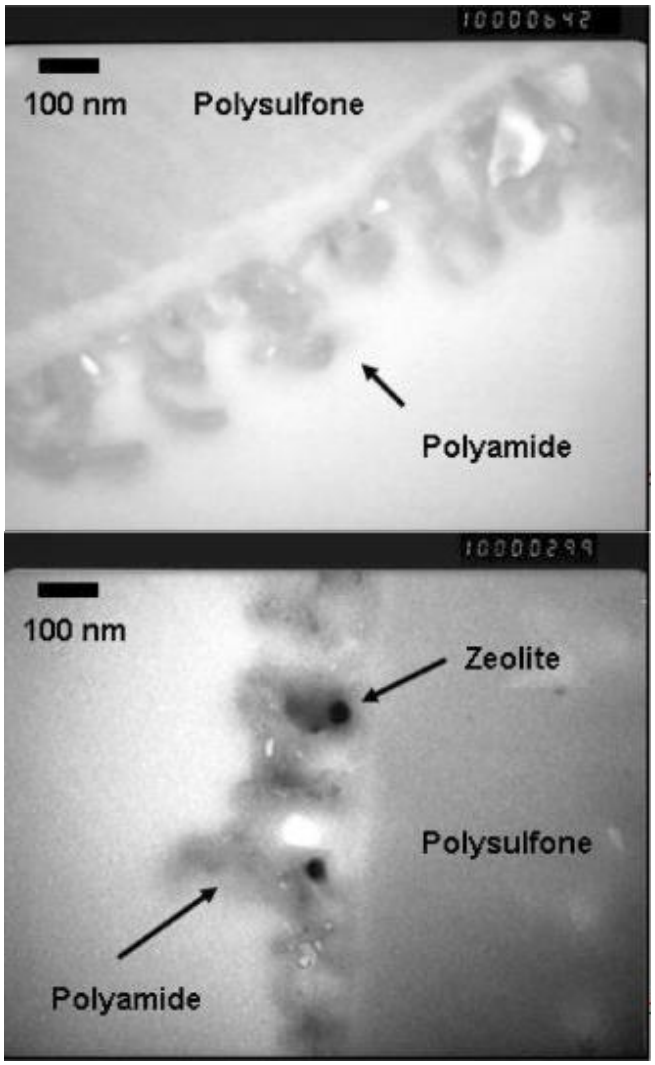
100 nm
Polysulfone
Polyamide
100 nm
Zeolite
Polysulfone
Polyamide

Figure 14

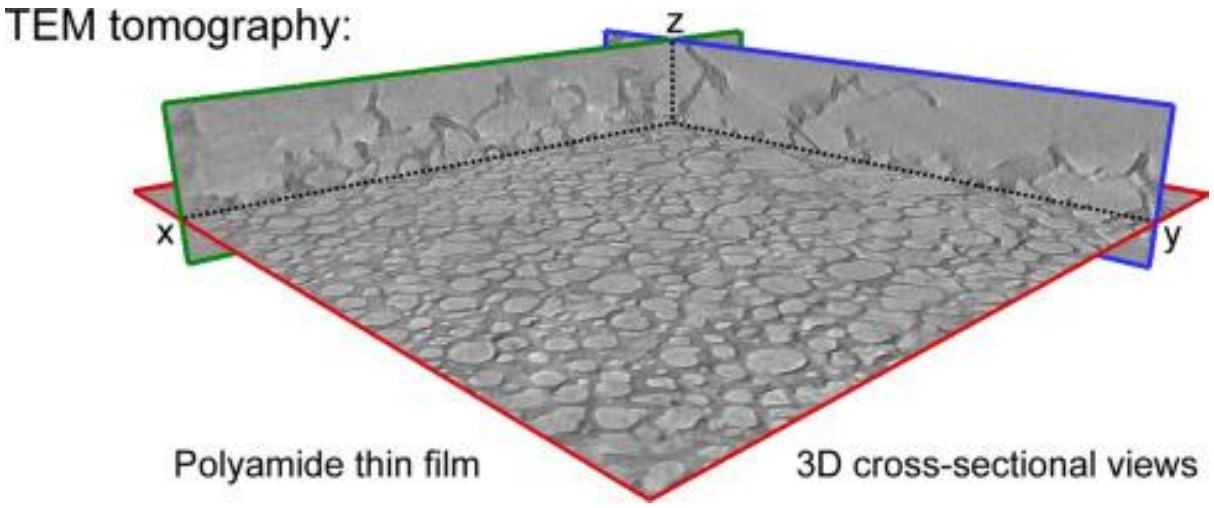
TEM tomography:
z
x
y
Polyamide thin film
3D cross-sectional views

Figure 15

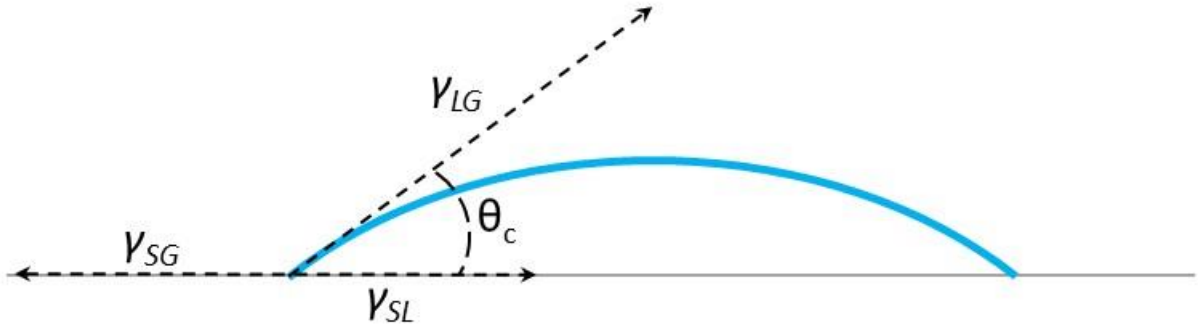

Figure 16

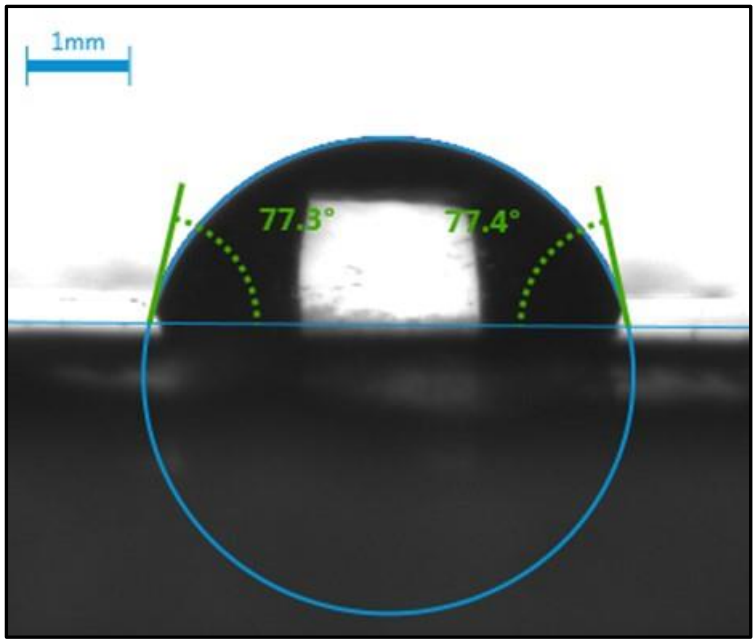

Figure 17

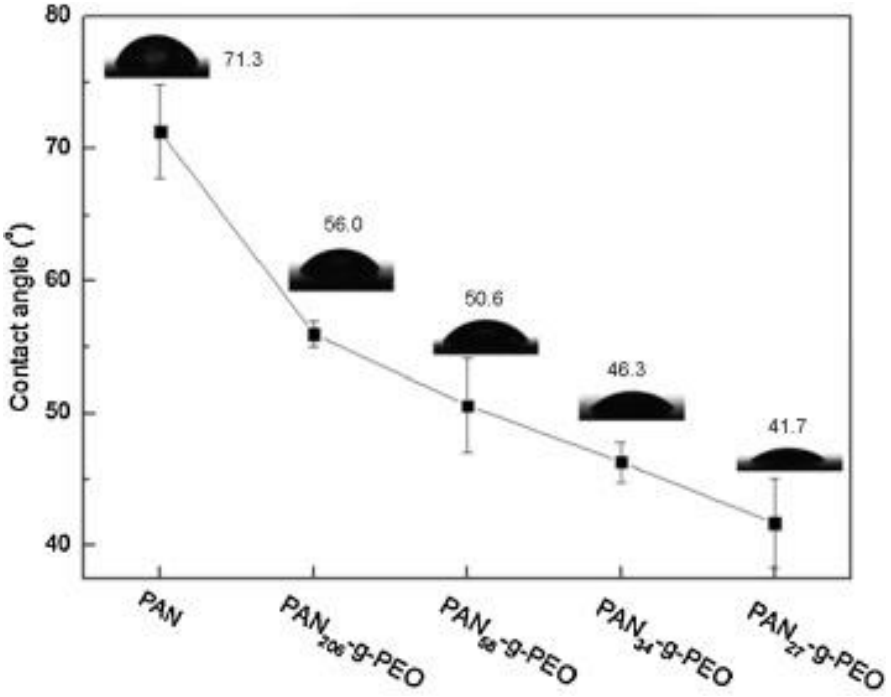
80
70
60
50
40
Contact angle (°)
71.3
56.0
50.6
46.3
41.7
PAN
PAN206-g-PEO
PAN68-g-PEO
PAN34-g-PEO
PAN27-g-PEO

Figure 18

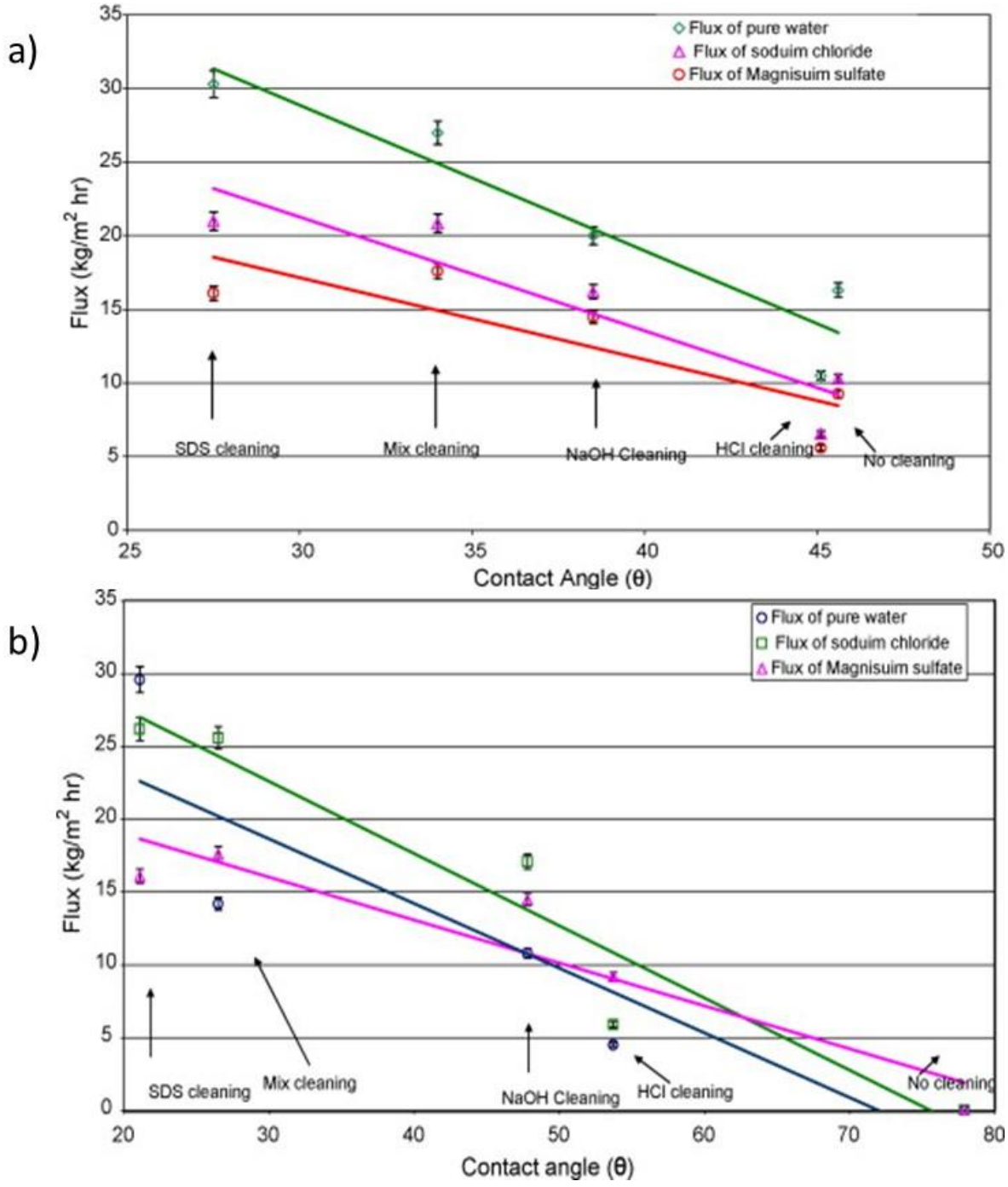
a)
Flux of pure water
Flux of soduim chloride
Flux of Magnisuim sulfate
Flux (kg/m2 hr)
SDS cleaning
Mix cleaning
NaOH Cleaning
HCl cleaning
No cleaning
Contact Angle (θ)
b)
Flux of pure water
Flux of soduim chloride
Flux of Magnisuim sulfate
Flux (kg/m2 hr)
SDS cleaning
Mix cleaning
NaOH Cleaning
HCl cleaning
No cleaning
Contact angle (θ)

Figure 19

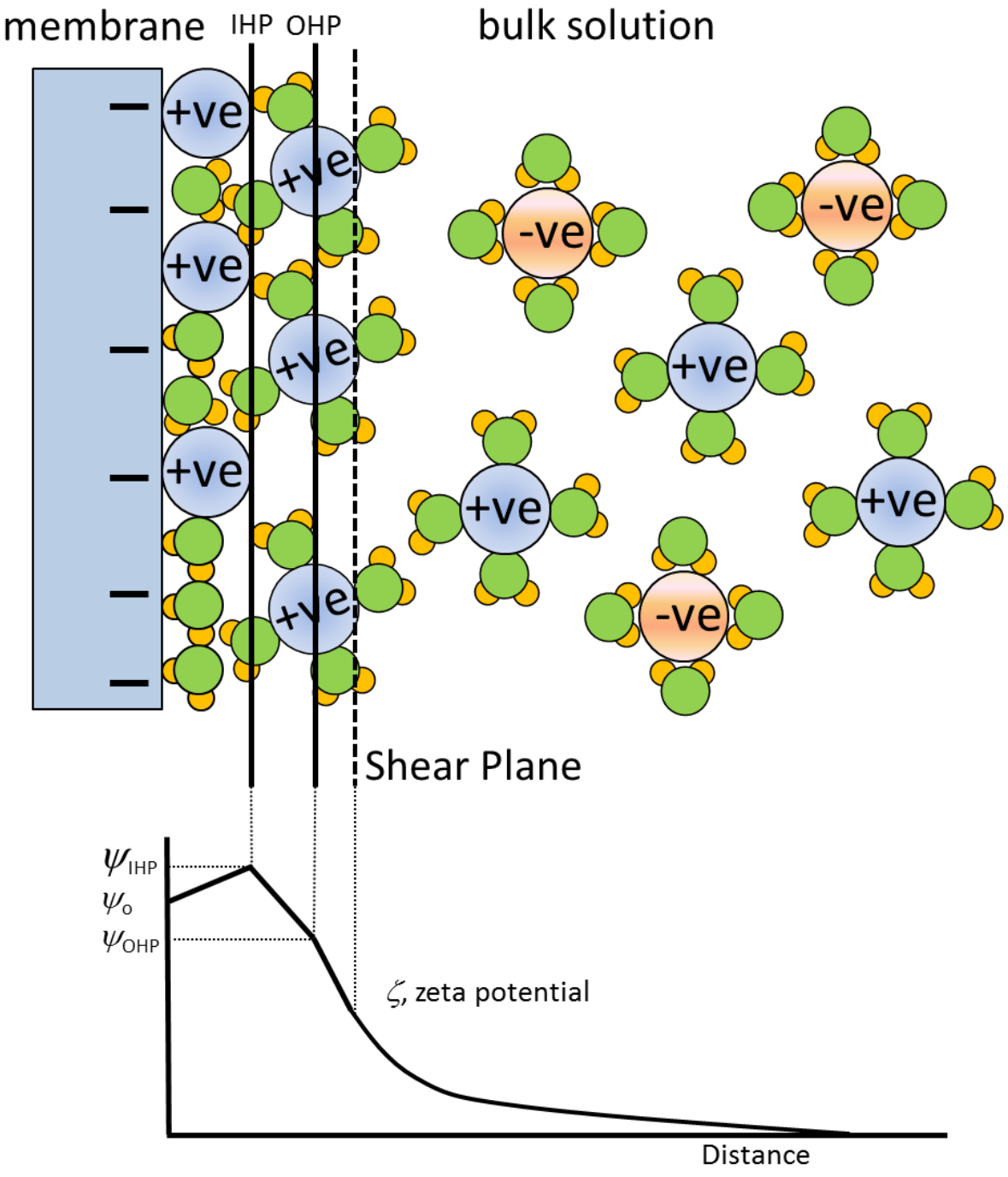
membrane
IHP
OHP
bulk solution
+ve
-ve
Shear Plane
ψ_{IHP}
ψ_o
ψ_{OHP}
ζ, zeta potential
Distance

Figure 20

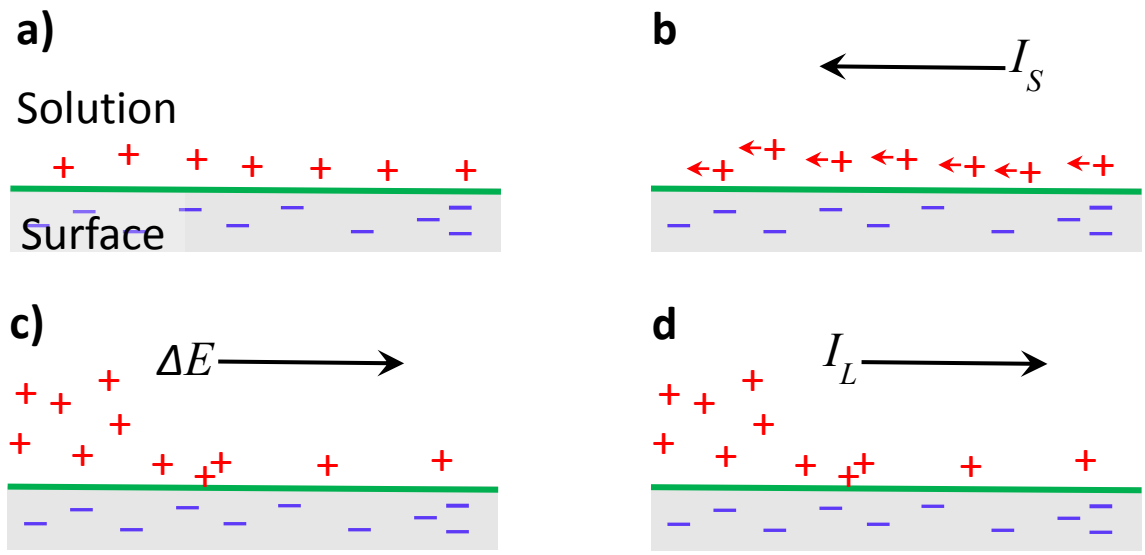

Figure 21

Technique	***Use in Membrane Characterisation***	***Advantages***	***Disadvantages***
Fourier Transform Infra-red Spectroscopy (FTIR)	Chemical characterisation of materials. Surface characterisation accessed with attenuated total reflectance (ATR) module.	Fast acquisition with high signal to noise ratio.	IR signal absorbed strongly by water.
Raman Spectroscopy	Chemical characterisation of materials. Various adaptations allow chemical scanning of surfaces	Can distinguish some functional groups insensitive to IR signal. High spatial resolution.	Raman signal weak leading to lower sensitivity than FTIR
Nuclear Magnetic Resonance Spectroscopy (NMR)	Determination of structure	Non-destructive. Simple sample preparation. Fast acquisition	Relatively insensitive compare with other techniques. Expen equipment. Mass limit for macromolecule (>30-40 kDa).
Electron Spin Resonance (ESR)	Determination of structure	Fast acquisition, high sensitivity, high specificity.	Specificity related to presence unpaired electrons – may not relevant to all materials, spin label may need to be added
X-Ray Photon Spectroscopy (XPS)	Chemical analysis of membrane surface	Very high chemical sensitivity. Non-destructive. Quantitative chemical and elemental information.	Slow processing. High vacuum required. Expensive equipmer
Small Angle Neutron / X-Ray Scattering (SANS/ SAXS)	Determination of structure	High spatial resolution.	Neutrons relatively insensitive matter.
Atomic Force Microscopy (AFM)	Quantitative measurement of surface topography and interaction forces	Can image in liquid. Quantitative height information and surface nano-mechanical properties can be measured. Surface interaction measurements between different materials accessible	Slow image acquisition. Lim sample height ra accommodated. Convolu effects at high resolu Maximum scan range typi 100 µm in *x, y* plane.
Scanning Electron	High resolution imaging of	Fast image acquisition time. Wide	Imaging of artefacts: non-

Microscopy (SEM)	membrane surfaces and cross-sections. Elemental analysis	field of view. Simultaneous surface elemental analysis obtainable with EDX unit.	conductive samples may requ metal coating. Imaging in vacuum.
Transmission Electron Microscopy (TEM)	High resolution imaging of membrane surfaces and cross-sections. Elemental analysis	Very high resolution obtainable. 3D tomography possible. Simultaneous surface elemental analysis obtainable with EDX unit.	Laborious sample preparation required. Metal coating of no conducting samples. Small fie view.
Contact Angle Measurement	Characterisation of surface wettability, surface free energy	Direct measurement of surface wettability. Can obtain information on surface free energy.	Porous membranes may caus problems using sessile drop method. Wilhelmy plate meth not suitable for asymmetric membranes
Streaming Potential Measurement	Characterisation of surface electrical properties	ζ-potential of membrane surfaces easily calculated from streaming potential.	Transverse measurements unsuitable for small pore size tangential measurement set-u needed instead
Electro-osmosis	Characterisation of surface electrical properties	ζ-potential of membrane surfaces easily calculated from electro-osmotic potential.	Some situations may require estimation of ratio of surface conduction to bulk conductivi (Dukhin number)
Sedimentation Potential	Characterisation of particle surface electrical properties	Can study more concentrated suspensions than electrophoresis. Visual measurements can be carried out simultaneously.	Can only measure particles. F membrane measurements sample needs to be fragment first. Slow measurement.
Electrophoresis	Characterisation of particle surface electrical properties	ζ-potential easily calculated from electrophoretic mobility of suspended particles	Can only measure particles. F membrane measurements sample needs to be fragment first

Table 1